Final report

Design of Electronic Properties of h-BN/Blue Phosphorene van Der Waals Heterostructure: First-Principles Study

Asst. Prof. Dr. Thanayut Kaewmaraya
Faculty of Science
Khon Kaen University

02/May/2020

MRG6180157

Final Report

Design of Electronic Properties of h-BN/Blue Phosphorene van Der Waals Heterostructure: First-Principles Study

Asst. Prof. Dr. Thanayut Kaewmaraya
Faculty of Science
Khon Kaen University

Project Granted by the Thailand Research Fund

Abstract

Project Code: MRG6180157

Project Title: Design of Electronic Properties of *h*-BN/Blue Phosphorene van Der Waals Heterostructure: First-Principles Study

Investigator: Asst. Prof. Dr. Thanayut Kaewmaraya

E-mail Address: Department of Physics, Faculty of Science, Khon Kaen University, Muang Khon Kaen, Khon Kaen, 40002
thakaew@kku.ac.th

Project Period: 02/05/2018 – 02/05/2020

Abstract:

Recent achievements of fabricating phosphorene, a quasi-single layer of phosphorus with the two-dimensional (2D) planar geometry, have attracted significant interests in devising high-performance (opto) electronics due to its semiconducting feature and ultrafast carrier mobility. Despite such benefits, phosphorene suffers from the rapid degradation in the ambient air to subsequently form insulating phosphorus oxides and eventually lost its profitable characters. On the basis of the *ab-initio* density functional theory (DFT), this research project presents the fundamental electronic and optical properties of the artificial BN-phosphorene van der Waals heterostructures (vdWHs) in which BN is exploited as both the protective layer and the electronic controller. The findings reveal that BN is a proper air-resistant layer because of the intrinsically weak vdW forces between BN and phosphorene sheets that negligibly perturb the host properties. Substitutional doping of carbon into BN can further modulate the electronic and optical properties of vdWHs to be used as promising solar absorbers with the upper bound of 22% theoretical conversion efficiency. Furthermore, the current project reports the potential functionality of phosphorene as chemical gas sensors. This material offers the exceptional selectivity and sensitivity for detecting toxic NO_2 even at the ultralow gas concentration of part-per-billion (ppb), surpassing the detectability of most conventional sensors based on transition oxides. The academic merit of this project is demonstrated by an obligatory international publication in Applied Surface Science (Q1, IF = 5.1) and this work was presented in an international conference. The other by-product publication is currently under review in Journal of Hazardous Materials (Q1, IF = 7.4).

Keywords: Phosphorene, Degradation, Gas sensors

Executive summary

Atomatically-thin 2D materials have played a disruptive role in materials science over the last couple of decades since the experimental debut of graphene in 2004 [1,2]. Up to present, such a considerable number of 2D crystals have been successfully created that the family of 2D materials could span the broad spectrum of solid properties ranging from insulators to superconductors [1]. This leads to a variety of major applications covering electronic and optoelectronic devices, biosensors, and energy storage and generation, to name a few [2,3]. Nevertheless, intensive attempts to fabricate new 2D materials remain on-going in order to achieve novel properties for enhancing certain functionalities. More novel 2D materials will be expectedly discovered in the near future [4].

As an alternative route, integration of existing ones has emerged as an innovative paradigm to produce 2D hybrids with unusual properties not available in the isolated components [5]. The occurrence of features stems from the superposition, intersection or cancelation of intrinsic quantum properties of the individuals [4]. Distinct 2D crystals can be assembled by two basic approaches, i.e., either lateral or vertical combination. The former requires the constituents to be lattice-matched, consequently limiting a number of eligible heterostructures. On the other hand, the latter does not necessitate the lattice-matching constrain because such heterostructures rely on the controllable vertical stacking of dissimilar layers between which weak van der Waals (vdW) interaction is primarily responsible for aggregation [6]. This scenario allows enormous combination of possibilities and the resulted hybrids are generally regarded as van der Waals heterostructures (vdWHs) [4]. The pioneering demonstration of vdWHs is fabrication of the graphene transistor on a BN substrate where the resultant transistor exhibited the improved performance (i.e., higher carrier mobility, reduced roughness, intrinsic doping and chemical reactivity) as compared to the traditional devices on SiO_2 [7]. Afterwards, generic vdWHs have become a feasible platform for both exploring fundamental physics and tailoring electronic and optical properties of 2D materials [4]. Notable examples include ballistic transport at a micrometer scale in graphene BN heterostructures [8], strong light-matter interaction in transition metal dichalcogenides (TMDCs)/graphene [9], valley-polarized excitons in WSe_2-$MoSe_2$ vdWHs [10], graphene/MoS_2 tunneling transistors [11], ultra-responsive photodetectors made from hybrid BN-2D black phosphorene [12,13]. In particular, the concept of vdWHs can resolve the so-called air-degradation of two-dimensional phosphorus [12,14].

Phosphorus can be found in various polymorphs (e.g., white, red, violet and black) among which black phosphorus is the most stable form. Although it was discovered over a century ago, mechanical exfoliation to become the few-layer form (named black phosphorene or BlackP hereafter) was recently realised in 2014 with the demonstration of the ambipolar field effect ensuing the exceptional performance in field effect transistors

(FETs) [15–17]. Unlike semi-metallic graphene, BlackP is a direct-gap semiconductor enabling the ultra-high drain current on-off ratio (~10^5) [15–17]. Its gap size also covers visible to near-infrared light spectrum [18] and it is adjustably thickness-dependent, ranging from 0.3 eV in bulk to around 1.73 eV in monolayer [19]. The topology of the direct band gap remains preserved regardless of thickness, unlike in TMDCs. Furthermore, two-dimensional phosphorus possesses the greater electronic transport (carrier mobility of 1000 cm^2/Vs at room temperature) which is also directionally anisotropic along the zigzag and arm-chair directions [16,20]. These exceptional features render BlackP to be an appropriate material for high-performance electronics and optoelectronic devices such as FETs, ultra-sensitive photodetectors, thermoelectric generators, and solar cells [19].

However, BlackP rapidly degrades to an insulating phosphorus oxide within a few hours under ambient conditions, consequently losing its overall attractiveness [14,21,22]. The severe oxidation process is basically attributed to the intrinsic wave-like crystal morphology and sp^3 bonding character [23]. Each phosphorus atom is covalently bonded with 3 neighbouring atoms, leaving the lone-paired electrons to be chemically prone to oxidation. This oxidative degradation can be circumvented by making vdWHs in which the atomically smooth and air-insusceptible BN is exploited as the protective layers. The use of BN is advantageous because of being a large-gap insulator (5.90eV) [24] with relatively less amount of dangling bonds and charge traps [7]. As a result, the environmental stability of BlackP in BN-BlackP vdWHs is prolonged yet its electronic properties remain unperturbed due to the weak vdW interaction [25]. Despite being the capping layer, one can further anticipate the novelty of BN-BlackP vdWHs when the protective material is substitutionally doped by C to form new BC_xN-BlackP (x=0, 2, and 6) hybrids. This concept is inspired by the compositional dependence on electronic properties of ternary borocarbonitrides (BC_xN) of which their band gaps get reduced gradually upon the increasing carbon concentration (from 5.90 eV in BN [24] to 0.98eV in BC6N) [26–29]. Hence, such vdW heterostructures of BC_xN and BlackP can be promising for two reasons, i.e., (i) retaining the air-stability of BlackP and (ii) permitting freedom to tune the electronic and optoelectronic properties of these vdWHs. The latter point is an intriguing space for further elucidation to enable targeted applications.

This work aims at unravelling the electronic and optical properties of BC_xN-BlackP (x=0, 2, and 6) bilayer van der Waals hybrids by means of first-principles density functional theory (DFT) calculations. The key fundamental properties, including band structures, chemical bonding, band alignments, and the variation of band offsets under the influence of external electric field of these hybrids are studied. Furthermore, the prospective exploitation of these vdWHs in solar cell applications is examined through computing the absorbance and subsequently estimating the solar power conversion efficiency. The findings manifest that the band alignment of BC_xN-BlackP vdWHs are the function of

carbon concentration and the external electric field (i.e., the tunable transition from type I to type II band offset at the appropriate concentration and field strength). In particular, type-II offset in BC_6N/BlackP can intensify solar absorption in the majority infrared regime, resulting in the exceptional photovoltaic performance.

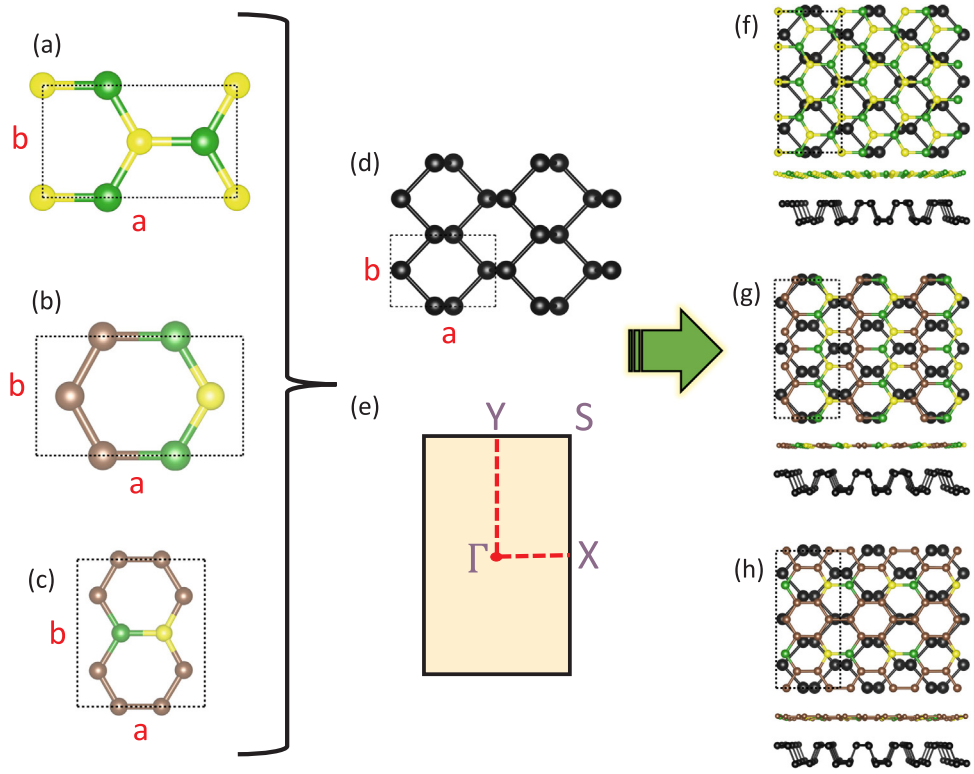

Fig. 1. Rectangular unit cell of monolayer (a) BN, (b) BC_2N, (c) BC_6N, and (d) BlackP. (e) First Brillouin zone of the orthorhombic symmetry with labeled high- symmetry points Γ(0.0, 0.0, 0.0), X(0.5, 0.0, 0.0), Y(0.0, 0.5, 0.0) and S(0.5, 0.5, 0.0). The unit cells as seen from the bird's eye and side views of (f) BN/BlackP, (g) BC_2N/blackP, and (h) BC_6N /blackP bilayer vdWHs. The boron, carbon, nitrogen and phosphorus atoms are represented by the green, brown, yellow, and black spheres, respectively.

Modelling of BC_xN-BlackP bilayer vdWHs was based on the original unit cells of BN, BC_xN [26], and BlackP. The cells of BN and BC_xN are hexagonal, whereas that of BlackP is orthorhombic. However, nominal rectangular unit cells were created to circumvent the lattice dissimilarity as shown in Fig. 1(a–d) with the orthorhombic first Brillouin zone shown in Fig. 1(e). The lattice constants of the unit cells representing (BN/BlackP), (BC_2N/BlackP), and (BC_6N/BlackP) heterostructures are (a = 4.571 Å, b = 9.927 Å, c = 30 Å), (a = 4.519 Å, b = 9.991 Å, c = 30 Å), (a = 4.593 Å, b = 9.901 Å, c = 30 Å) as displayed in Fig. 1(f–h). Although these cells internally impose the infinitesimal in-plane strain to BC_xN and BlackP sheets, the use of such lattice parameters is physically valid. This is because the computed band alignments of isolated BC_xN and BlackP in

these sets of rectangular cells resemble those of the original cells. Note that the fictitious strain is an unavoidable theoretical artifact in building vdWHs to minimise the strain. However, it is not required in real devices owing to the weak vdW interaction between the monolayers [30]. The optimal interlayer distances between the monolayers were estimated by fitting the binding energy (E_b), $E_b = E_{BC_xN-BlackP} - \left(E_{BC_xN} + E_{BlackP}\right)$ as a function of the interlayer distance (r) to Lennard-Jones (LJ) potential, $U_{LJ} = 4\varepsilon\left[\left(\frac{\sigma}{r}\right)^{12} - \left(\frac{\sigma}{r}\right)^{6}\right]$, where ε and σ are the fitting parameters. The first term in LJ potential accounts for repulsion, whereas the second term describes attraction. Different stacking patterns of each BC_xN-BlackP were considered and the structures with the lowest binding energies have been subsequently chosen for further investigation. DFT-based *ab-initio* calculations were performed using VASP code [31]. The exchange correlation energy was treated by the gradient corrected approximation according to Perdew Burke-Ernzerhof (PBE) formalism [32]. Weak vdW interaction between BC_xN and BlackP sheets was considered by incorporating the pairwise dispersive correction in the Kohn-Sham energies using the DFT-D3 approach [33,34]. The energy cutoff for the plane-wave basis set was set to 500 eV. The first Brillouin zone was sampled by Monkhorst-Pack scheme with k-mesh of 15x7x1 and 17x9x1 for structural optimisation and optical absorption, respectively. Structural optimisation was satisfactorily terminated when Hellmann-Feynman forces exerting on each atom were less than 10 meV/Å. The tolerance of electronic self-consistency cycle was set to 1 x 10^{-6} eV. The accurate determinations of band structures and optical absorption of the selected systems were carried out using hybrid Heyd-Scuseria-Ernzerhof (HSE06) functional [35,36]. However, the findings presented here were obtained from PBE functional, unless stated otherwise.

Results and discussion

1. Interlayer binding energies of vdWHs

Fig. 2(a) shows the interlayer binding energies of vdWHs as a function of the interlayer spacing. The optimal distance of BN-BlackP is 3.53 Å with a minimum binding energy of 25.95 meV/atom. These values are consistent with the reported theoretical findings in spite of the insignificant deviation inherited from the dissimilar approaches used to describe vdW forces [25,37]. The weak magnitude of binding energy and the long interlayer distance manifest the principal role of vdW interaction caused by the instantaneous dipole from charge fluctuation. The obtained fitting parameters ε and σ according to LJ formalism are 24.95 meV/atom and 2.95 Å, respectively [25]. This interlayer binding energy is slightly weaker than the measured value of graphite (30.4 meV/atom [38]), implying its relative exfoliation energy with respect to graphite. Furthermore, the binding energy as a function of the interlayer spacing allows us to

estimate the elastic constant (C_{33}) in the perpendicular direction of BN and BlackP interface using the following expression, $C_{33} = \frac{r_0}{A}\frac{\partial^2 E_b(r)}{\partial r^2}$, where r_0 is the equilibrium interlayer distance, A represents the in-plane surface area of the vdWH supercell and E_b is the binding energy. The calculated C_{33} is 33.10 GPa, slightly less incompressible than that of graphite, 36.50 GPa [39]. The reason can be attributed to the fact that the wave-like geometry of BlackP results in the large flexibility along both the horizontal and the vertical directions [25].

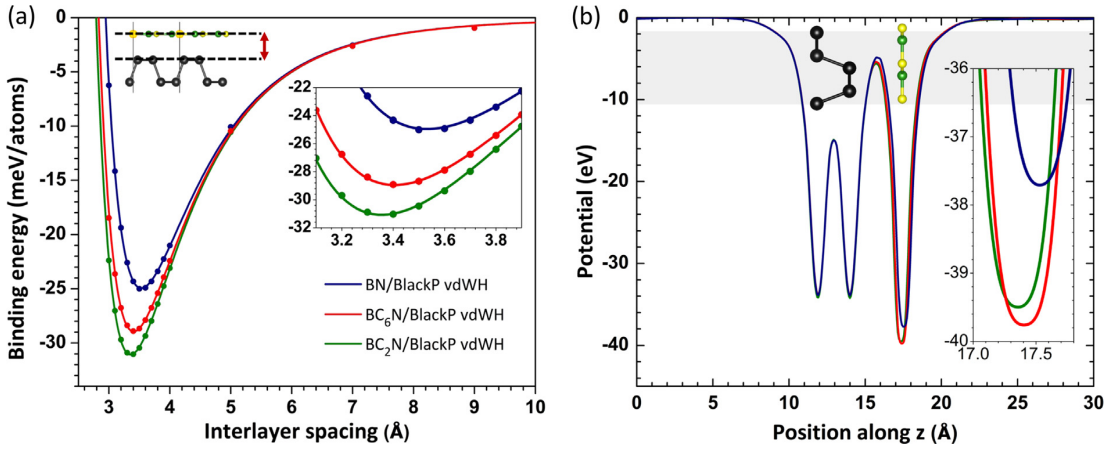

Fig. 2. (a) Interlayer binding energy (E_b) per atom of BC_xN-BlackP vdWHs as a function of the interlayer spacing which is defined as the difference in spatial coordinates in c direction between the top-most atom of BlackP and the bottom-most atom of BC_xN. The inset magnifies E_b close to the optimal points. (b) The plane- average potential along the vertical interface between BC_xN and BlackP and the inset which enlarges the potentials of BC_xN near the minimum points.

Meanwhile, the presence of substitutional carbon dopants in BN relatively decreases the interlayer distances, leading to the increase in binding energies despite the non-monotonic trend. The equilibrium distances (maximum binding energies) of BC_2N-BlackP and BC_6N-BlackP vdWHs amount to 3.37 Å (-30.195 meV/atom) and 3.43 Å (-27.860 meV/atom), respectively. The calculated binding energies are quantitatively comparable to that of graphite, reflecting that the peeling (exfoliation) energies of these hybrids are of nearly the same strength. The fitting parameters $\mathcal{E}$ and σ of BC_2N-BlackP (BC6N-BlackP) hybrid are -31.083 (-28.950) meV/atom and 2.79 (2.83) Å, respectively. The estimated C33 elastic constant of BC_2N-BlackP (BC_6N -BlackP) hybrid is 42.70 (36.20) GPa, indicating that the addition of carbon atoms makes the vdWHs less compressible. Furthermore, Fig. 2(b) depicts the plane-average potential (V_{ave}) which basically describes the combination of Hartree ($V_{Hartree}$), exchange-correlation (V_{xc}), and external (V_{ext}) potentials. Apparently, there are potential drops across the interfaces to

create the built-in electric fields between the constituent sheets, yielding the spontaneous polarisation [40]. These intrinsic fields are triggered by the fundamental differences in electronegativity of B(2.01), C(2.50), N(3.07) and P(2.06) atoms and they point from BlackP to BC_xN resembling our previous work of BC_xN-Blue phosphorene interface [41]. Hence, the excitonic behaviour of vdWHs (i.e., the optical properties) tends to differ from that of individual quasi-monolayer BlackP and BC_xN due to the typically reduced dielectric screening in 2D materials [16].

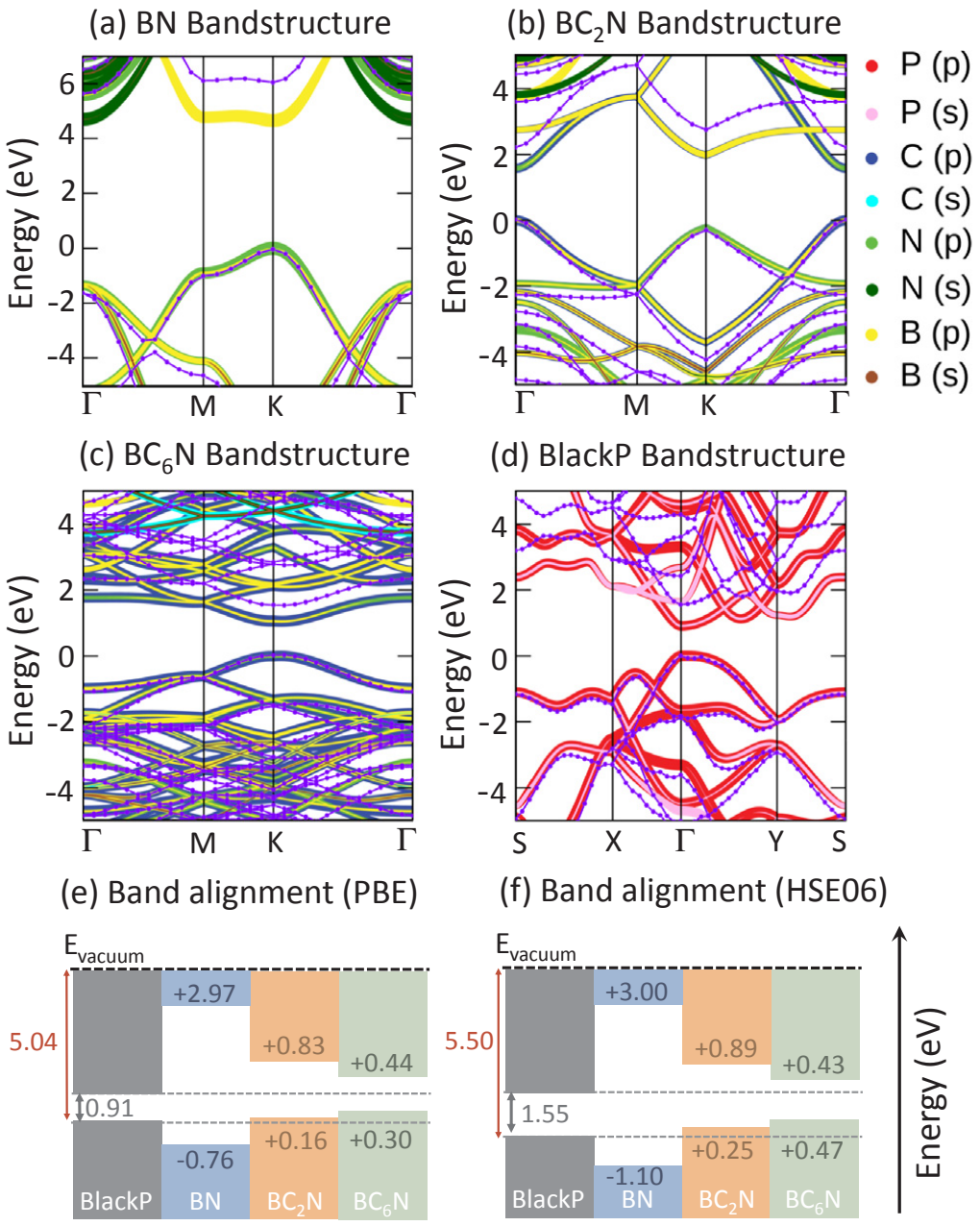

Fig. 3. Orbitally-resolved band structures of (a) BN, (b) BC_2N, (c) BC_6N, and (d) BlackP where the Fermi level is set to zero. The solid violet lines represent band dispersion calculated by HSE06 functional. Band alignments calculated by (e) PBE and (f) HSE06

functionals in which the Fermi energies are referenced to the vacuum level. The red numbers denote the calculated work functions.

2. Electronic structures

Fig. 3(a–d) depicts the orbitally-resolved band structures of BlackP, BN, BC_2N, and BC_6N as calculated by PBE and HSE06 levels of theory. The band gap of BlackP by PBE (HSE06) is 0.91 (1.55) eV. The HSE06 gap agrees with the reported DFT calculations [25,42,43] and close to the experimental value of 1.73 eV [44]. In particular, BlackP shows a direct-gap feature at Γ. Both the valence and conduction band extrema are formed by P-$3p_z$ orbital where the band curvature (i.e., carrier effective masses) along $\Gamma - X$ greatly differs from that along $\Gamma - Y$. This indicates that π bands derived from interactions between P-$3p_z$ orbitals contribute to direction-dependence and exceptional carrier mobility of this 2D phosphorus. On the other hand, BN is a huge band gap (direct) insulator at K with the calculated gap of 4.65 (5.65) eV by PBE (HSE06), of which the HSE06 gap is slightly smaller than the experimental value of 5.91eV [24]. The valence and conduction band edges are predominantly contributed by π bands from N-$2p_z$ and B-$2p_z$, respectively. The dispersion of conduction band along $M - K$ is virtually flat. This scenario leads to the difficulty in unambiguously classifying BN as either a direct-gap or an indirect-gap insulator owing to the influential role of immense excitonic binding energy in the absorption onset [24]. Meanwhile, it is found that substitutional doping of carbon in BN drastically reduces the gap. The band structure of BC_2N attests the semiconducting character with a direct PBE (HSE06) gap of 1.60 (2.19) eV at the zone center. In particular, the edge states are σ bands derived from the enhanced planar overlap between B-$2(p_x + p_y)$ and C-$2(p_x + p_y)$ for the valence band edge and N-$2(p_x + p_y)$ and C-$2(p_x + p_y)$ for the conduction band edge. This results in the significant drop in the gap at Γ. Nevertheless, the band edges at K, like BN, still show π-character where the valence (conduction) band extremum is contributed by N-$2p_z$ (B-$2p_z$). At higher doping concentration, BC_6N possesses the cone-like direct PBE (HSE06) gap of 1.04 (1.51) eV at K, whereas its Γ-gap is considerably greater. This is attributed to the fact that BC_6N is in the heavily doped regime where its band structure approaches that of graphene. The HSE06 gap of BC_6N suitably falls into the infrared region which is the majority of solar spectrum. Moreover, our spin-polarised calculations assure that BC_2N and BC_6N are nonmagnetic. This is because the simultaneous replacement of B and N sites by C atoms within the interaction length (around 10 Å) eradicates spin-splitting of the impurity states to adopt the S =0 configuration [45].

The band gaps of BC_xN do not only drop with the increasing carbon concentration, but their band edge positions also get changed accordingly. This further motivates us to elucidate the band alignment when they actually form vdWHs with BlackP. Fig. 3(e–f) show the PBE and HSE06 band alignment diagrams of the isolated BC_xN and BlackP

prior to forming vdWHs. The alignment is obtained by calculating the work functions of materials (W), $W = E_{vac} + E_F$, where E_{vac} and E_F represent the vacuum level and the Fermi energy, respectively. The diagrams imply that the formation of BN-BlackP vdWH yields straddling type-I band offset [25]. On the contrary, BC_xN-BlackP composites adopt type-II band offset. The band alignments from PBE and HSE06 are similar despite the differences in the gaps and work functions, manifesting that relative band alignments are less functional dependent [46]. Notably, the valence band offsets between BlackP and BC_xN are infinitesimal that the prominent interlayer couplings when forming vdWHs potentially alters the offsets.

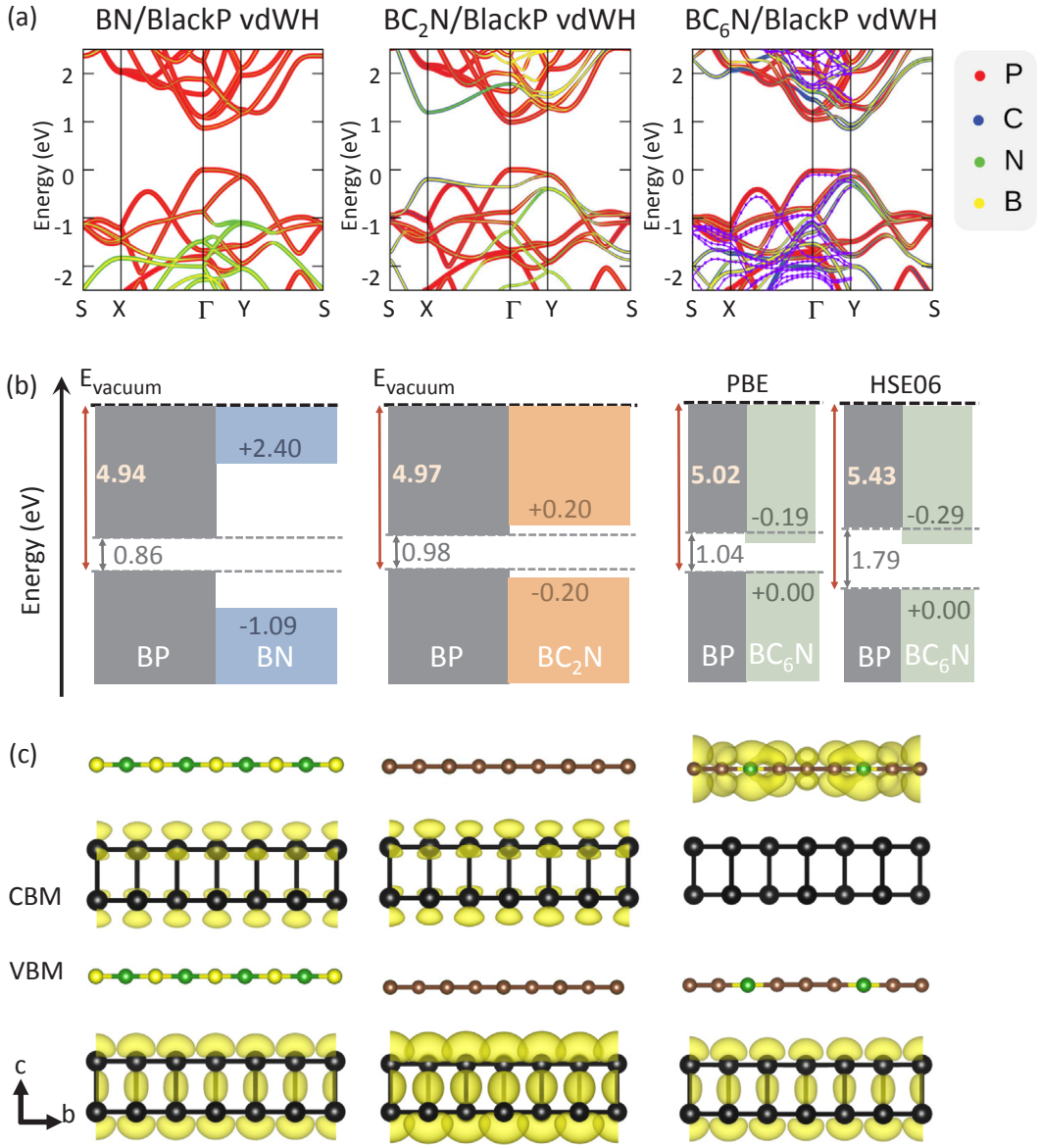

Fig. 4. (a) Projected band structures of BC_xN/BlackP vdWHs. The solid violet lines represent band dispersion calculated by HSE06 functional. Here, the valence band maximum has been shifted to zero energy. (b) The band alignment diagram and (c) the charge density of valence and conduction band edges.

Fig. 4(a–c) show the projected band structures, the band alignment diagram, and the charge density of valence and conduction band edges of BC_xN-BlackP vdWHs. It is evident that BN-BlackP and BC_2N-BlackP hybrids form type-I band alignment, while BC_6N-BlackP differently adopts type-II. Intriguingly, the band alignment of BC_2N -BlackP vdWH differ from that in Fig. 3(e–f). Moreover, the valence and conduction band edges of BC_6N-BlackP are now populated by BlackP and BC_6N, respectively, differing from the prior band positions in Fig. 3(e–f). The valence bands of BlackP and BC_6N in the vdWH now equalises because of the overlap among P-$3p_z$, N-$2p_z$, and C-$2p_z$ orbitals. In particular, BC6N-BlackP exhibits type-II offset at Y-point which is preferable for optoelectronics and photovoltaics because of the spontaneously spatial separation of electrons and holes [47,48]. Further calculations of band structure and band alignment by HSE06 also yield the similar band alignment despite the difference in the gap and the offset magnitude (the conduction band offset of 0.19 eV by PBE and 0.29 eV by HSE06). It is intriguing to highlight that high hole mobility in BlackP remains preserved in the BC_2N-BlackP and BC6N-BlackP heterobilayers, as their VBM are contributed by BlackP [60]. It should be emphasised that the band realignments of BC_2N-BlackP and BC_6N-BlackP vdWHs compared with those of their isolated components are because the presence of carbon atoms intensifies the charge transfer from BlackP to BC_xN. This is apparently ascertained by the charge difference plot in Fig. 5(a). There is charge accumulation (cyan) and depletion (yellow) on BC_xN and BlackP, respectively, simply because of the differences in electronegativity. Consequently, the built-in electric field gets maximised and the band positions of BlackP and BC_2N are shifted accordingly. Hence, we conclude that the built-in electric fields play a major role in the band alignment of vdWHs, especially the vdWHs constituted by the sheets with the striking difference in the electronegativities.

3. Effect of the electric field

Numerous studies have revealed that electronic properties of devices based on vdWHs are effectively gate-tunable (i.e., the application of back gate voltage) due to Stark effect [49,50]. The modulation of electronic and optical properties by the external electric field is beneficially reversible and non-invasive, unlike the irreversible chemical doping approach. Hence, it is intriguing to explore how BC_xN-BlackP vdWHs respond to the perturbative electric field for the possible realisation of electronic devices. Fig. 5(b-c) displays the charge differences of vdWHs under the in fluence of the positive and negative electric fields of ± 0.5 eV/Å where the direction of positive electric field is +c and vice versa. The presence of perturbation clearly causes the spatial charge redistribution. Specifically, the positive electric field induces more charge transfer from BlackP to BC_xN because the external field constructively superimposes on the built-in. Meanwhile, the negative field suppresses the charge transfer because the external field destructively reverses the built-in. More insights into the variation of band gap (E_g) of vdWHs as a function of the time independent electric field strength is shown in Fig. 5(d). Despite the

different trends, the heterostructures undergo the semiconductor-to-metal transition at the same critical field magnitudes in both the directions, around -0.8 (+0.6) eV/Å for the negative (positive) bias. This is because their band gaps and Fermi energies of are nearly similar. Quantitatively, the PBE gaps (Fermi energies) of BN-BlackP, BC_2N -BlackP, and BC_6N -BlackP are 0.86 (-1.986), 0.98 (-1.896), and 0.85 (-1.986) eV, respectively. The phase transition facilitates the enormous tunnel current during the appropriate bias, whereas the current is comparatively less in the lack of bias, leading to the on-off ratio. In terms of the trends, the gap of BN-BlackP vdWH exhibits the plateau in the range -0.6 to +0.6 eV/Å where the band gap is field-independent. Unlike BN-BlackP, the reduction in band gaps of BC_2N-BlackP and BC_6N-BlackP hybrids exhibits the asymmetric quadratic Stark effect regardless of the direction, resembling the gate tunability in few-layer black phosphorus [50] and BlackP-MoS_2 vdWH [48].

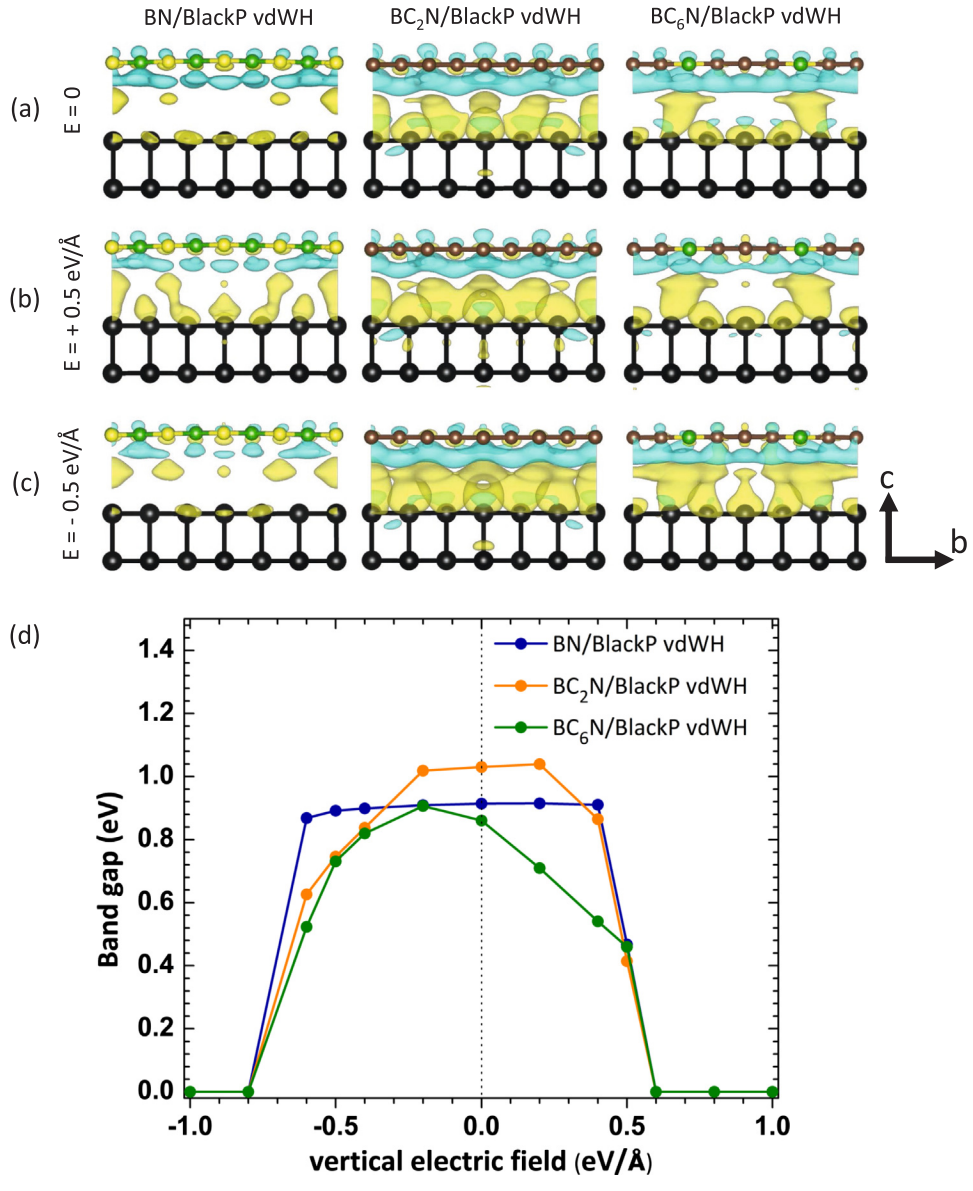

Fig. 5. The charge density difference (ρ_{diff}), $\rho_{diff} = \rho_{BC_xN-BlackP} - \left(\rho_{BC_xN} + \rho_{BlackP}\right)$ of vdWHs of (a) E-field = 0.0 eV/A , (b) E-field = +0.5 eV/A, and (c) E-field = -0.5 eV/A. The direction of positive electric field is +c and vice versa. Cyan and yellow colors represent charge accumulation and depletion, respectively. The isosurface level is set to be 0.0002 e/A^3. (d) Variation of band gap of BC_xN/BlackP vdWHs with respect to the vertical electric field (E-field).

The changes in the gaps of vdWHs under the influence of electric field rely on the positions of band edges. Fig. 6 shows the responsive trace of the band edges of BC_2N-BlackP and BC_6N-BlackP under the influence of the electric field from 0 to ±0.4 eV/Å. The findings reveal that the frontier states behave differently, depending on the high symmetry directions of the first Brillouin zone. The band edges of BlackP in all the vdWHs are not responsive to the field. On the other hand, the frontier states formed by BC_2N and BC_6N (i.e., $2p_z$ orbitals of B, C, and N atoms) are sensitively shifted towards each other. As a result, the band alignment of BC_2N-BlackP can be transformed from type-I to type-II at ±0.4 eV/Å. Likewise, type-II offset of BC_6N-BlackP is converted into type-I at ± 0.2 eV/Å, regardless the field direction. The findings indicate that the tunability of both band gap and band alignment of BC_xN-BlackP vdWHs is governed by the active responses of the 2pz orbitals from BC_xN. The different responsiveness of the edge states of BC_2N and BC_6N compared with those of BlackP can be ascribed to the lifting degeneracy by the Stark effect. The greater responsiveness of the edge states of BC_2N and BC_6N is associated with their edges states which are formed by B-$2p_z$ and N-$2p_z$ and C-$2p_z$ orbitals, unlike the frontier states of BlackP which are derived from the combination of $3p_x$, $3p_y$, and $3p_z$. Consequently, the enhanced diffuse nature of the p_z orbital readily facilitates greater charge redistribution (i. e., splitting of energy levels) [59]. This envisages the effective gate-tunability of these vdWHs as a building block in nanoelectronics.

4. Optical absorption and the photovoltaic performance of BC_6N-BlackP vdWH

BC_6N-BlackP vdWH exhibits type-II band offset that is feasible for spatial charge separation in the photovoltaic application. One can elucidate the performance of the photovoltaic device based on this vdWH by computing solar absorption. Fig. 7(a) shows the absorption of BC_6N-BlackP vdWH, BC_6N, and BlackP. Particularly, there is the relative enhancement in absorption of vdWH at the energy around 1.50–1.80eV compared to the independent components. The improvement is derived from the valence-to-conduction transitions from P-$3p_z$ to P-$3p_z$ at Γ and N-$2p_z$ to B-$2p_z$ at Y, see also Fig. 4(a). This is the manifestation of BC_6N/BlackP vdWH as the potential light absorber to attain more infrared lights, potentially leading to the efficient solar-to-electricity conversion. The amplified absorption further propels us to compute the power conversion efficiency (PCE,

η). This quantity describes the amount of solar energy being converted to electricity and it can be theoretically estimated according to Bernadi and Scharber formalism [51,52]

$$\eta = \frac{FF \cdot V_{OC} \cdot J_{SC}}{P_{light}} = \frac{0.65(E_g^d - \Delta E_C - 0.3)\int_{E_g^d}^{\infty} \frac{P(\hbar\omega)d(\hbar\omega)}{\hbar\omega}}{\int_{E_g^d}^{\infty} P(\hbar\omega)d(\hbar\omega)}$$

where FF is the fill factor which determines ratio between the maximum power point and the open circuit voltage and the short circuit current [53]. FF typically varies from 0.50 to 0.82, depending on materials, while FF is set to 0.65 in this study [52]. This empirical number is experimentally estimated according to the practical limit of external quantum efficiency of solar cells absorbing photon energies equal or greater than the donors' band gaps without the recombination losses [52]. Meanwhile, V_{OC} defines the estimation of highest open circuit voltage which is expressed as $V_{OC} = E_g^d - \Delta E_C - 0.3$ (in unit of eV). E_C d represents the optical band gap of the donor (here BlackP) which is regarded as the material with the relatively higher conduction band. ΔE_C accounts for the conduction band offset between the donor and the acceptor and the empirical factor 0.3 denotes the energy conversion kinetics. The optical band gap in the present study is approximated by the electrical band gap (i.e., Kohn-Sham band gap) at HSE06 level of theory. Although both kinds of band gap differ by the presence of exciton energy that generally makes the former smaller [54], this simplification remains reasonable due to the linear variation of exciton energy with the band gap [55]. The trend of PCE can be correctly predicted despite the systematic shift of the absolute values. J_{SC} is the short circuit current which is calculated by the integral of the energy dependence of AM1.5 solar energy flux,$P(\hbar\omega)$ in unit of W/m^{-2}/eV^{-1}, weighted by photon energy $\hbar\omega$. Meanwhile, Plight in the denominator is the total solar power of AM1.5 solar energy flux. The integrals of JSC and Plight were carried out by the basic Simpson approach. The comprehensive analysis of Eq. (1) tells us that either a too high or too small donor gap results in the low PCE. In addition, large E Δ retards PCE because of the thereby significant energy loss.

Fig. 7(b) depicts the dependence of the calculated PCE as a function of the conduction band offset (0.29 eV) and the band gap of the donor material (1.79 eV). BC_6N/BlackP vdWH can deliver the maximum PCE of around 22.0%, denoted by the hexagonal dot. In comparison, the experimental optical band gap taking excitons into account is 1.30 ± 0.02 eV [54] is estimated to be ca. 20.0%, denoted by the triangular dot. Considering the errors in calculating the donor's band gap is around 0.49 eV and the error in the open-circuit voltage (ΔV_{OC}) is 0.10 eV [51]. The error of PCE (α) can be evaluated as [51].

$$\alpha = \frac{1}{\eta}\sqrt{\left[\left(\frac{\partial\eta}{\partial V_{OC}}\right)\Delta V_{OC}\right]^2 + \left[\left(\frac{\partial\eta}{\partial E_g^d}\right)\Delta E_g^d\right]^2}$$

The error is calculated to be 3.0%, hence the upper bound of PCE ranging from 19.0 to 22.0%. This exceptional number is exceedingly comparable to the theoretical figures of several vdWHs such as 18.0% of BlackP-MoS_2 [48] and 23% of BAs-BlackP (high-throughput screening) [30]. The conceptual demonstration of using this vdWH as a solar absorber is schematically shown in Fig. 7(c). It should be mentioned that the theoretical PCE is solely based on the band gap and the conduction band offset. The actual PCE involves multiple factors such as transport of charge carriers, diffusion length and excitonic recombination, etc., which are not taken into account in the present work. In addition, PCE is probably less sensitive to the stacking pattern of the constituents of vdWHs because the intrinsically weak magnitude of interlayer interaction generally causes the minor changes in the atomic structures (and band gaps) of the component materials [56–58] Nonetheless, our proposed system can hopefully stimulate further in-depth investigation to entail the opportunity in alternative solar cell devices.

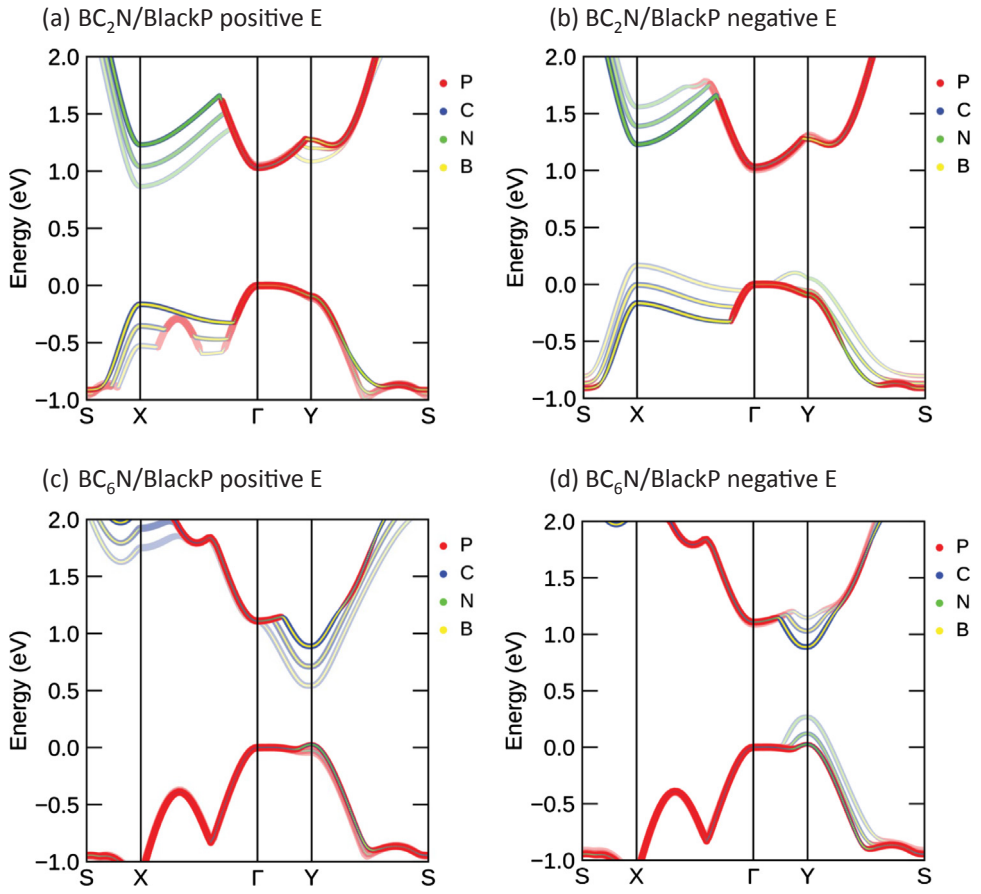

Fig. 6. (a) Relative variation of valence and conduction band edges of BC_2N/BlackP vdWHs with respect to the vertical electric field (a) BC_2N/BlackP with the field magnitude of 0.0, 0.2 and 0.4 eV/A° (b) BC_2N/BlackP with the field magnitude of 0.0, -0.2 and -0.4

eV/Å, (c) BC_6N/BlackP with the field magnitude of 0.0, 0.2 and 0.4 eV/Å, and (d) BC_6N /BlackP with the field magnitude of 0.0, -0.2 and -0.4 eV/Å.

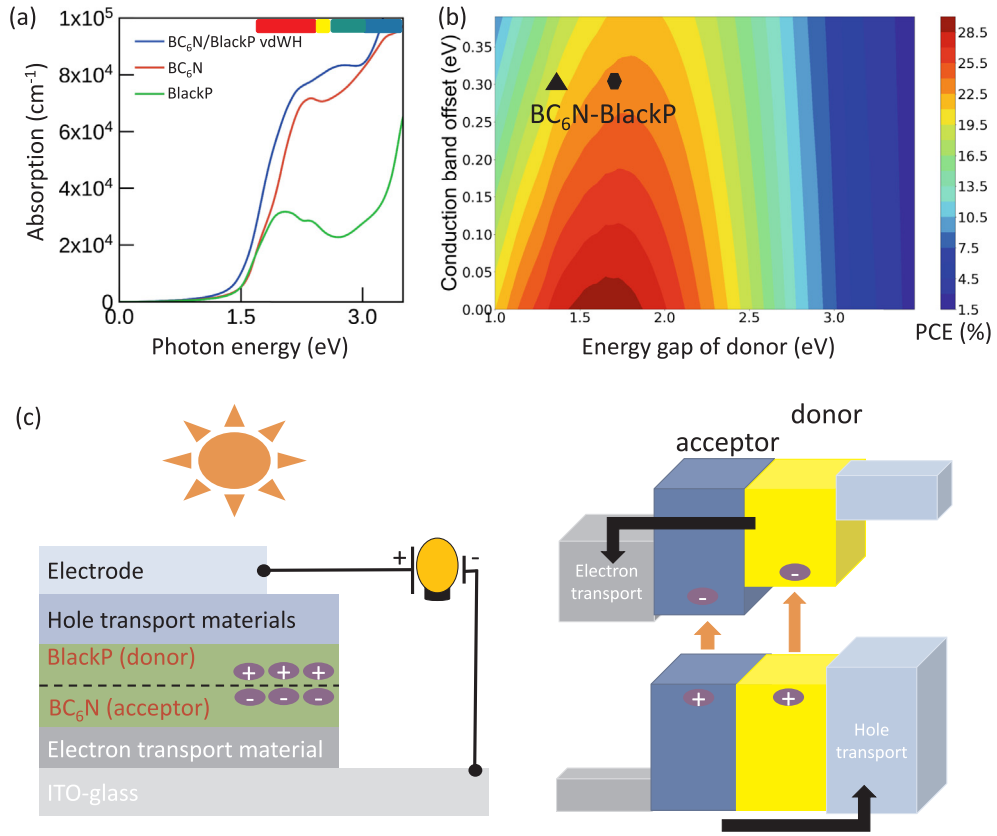

Fig. 7. (a) Absorption of BC6N/BlackP vdWH, (b) the landscape of the power conversion efficiency (PCE) as a function of the conduction band offsets and the band gap of the donor material. The hexagonal and triangular dots represent the theoretical PCE evaluated from the electronic HSE06 and the experimental optical gap, respectively. (c) the conceptual demonstration of the solar cell made from BC_6N/BlackP vdWH.

Conclusion

In summary, we present the electronic and optical properties of BC_xN-BlackP (x =0, 2, 6) vdWHs investigated by means of first-principles principles DFT. The electronic properties of these vdWHs are effectively tunable by varying carbon concentration. BN-BlackP and BC_2N-BlackP exhibit type-I band offset whereas BC_6N-BlackP adopts type-II band offset. The variation in band alignment is ascribed to the reduction in band gaps of BC_xN upon increasing carbon concentration and the prominent interlayer interactions between the constituent monolayers. The electronic properties of vdWHs can also be modulated by the external electric field due to the fundamental Stark effect. The band gaps of these hybrids drop with the applied electric field regardless of the field direction where band alignment also gets changed. This unique modulation in gap and alignment essentially enables gate-tenability of these vdWHs as a building block in electronic FET devices. Moreover, the potential photovoltaic application of BC_6N-BlackP vdWH has been investigated because of its type-II band alignment. BC_6N BlackP vdWH enhances solar absorption in the infrared region that leads to the efficient solar-to-electricity conversion. The estimated maximum power conversion efficiency (PCE) is exceptional 19.0–22.0%. This appealing figure can hopefully stimulate experimental studies to entail the opportunity in alternative solar cell devices

References

[1] G.R. Bhimanapati, et al., ACS Nano 9 (2015) 11509–11539.

[2] A.C. Ferrari, et al., Nanoscale 7 (2015) 4598–4810.

[3] N. Briggs, et al., 2D Mater. 6 (2019) 022001.

[4] C.N.R. Rao, U.V. Waghmare, 2D Inorganic Materials beyond Graphene, WORLD SCIENTIFIC (EUROPE), 2017.

[5] D. Jariwala, A.R. Davoyan, J. Wong, H.A. Atwater, ACS Photonics 4 (2017) 2962–2970.

[6] A.K. Geim, I.V. Grigorieva, Nature 499 (2013) 419–425.

[7] C.R. Dean, A.F. Young, I. Meric, C. Lee, L. Wang, S. Sorgenfrei, K. Watanabe, T. Taniguchi, P. Kim, K.L. Shepard, J. Honel, Nat. Nanotechnol. 5 (2010) 722.

[8] A.S. Mayorov, R.V. Gorbachev, S.V. Morozov, L. Britnell, R. Jalil, L.A. Ponomarenko, P. Blake, K.S. Novoselov, K. Watanabe, T. Taniguchi, A.K. Geim, Nano Lett. 11 (2011) 2396–2399.

[9] L.Britnell,R.M.Ribeiro,A.Eckmann,R.Jalil,B.D.Belle,A.Mishchenko,Y.-J.Kim, R.V. Gorbachev, T. Georgiou, S.V. Morozov, A.N. Grigorenko, A.K. Geim, C. Casiraghi, A.H.C. Neto, K.S. Novoselov, Science 340 (2013) 1311–1314.

[10] P. Rivera, K.L. Seyler, H. Yu, J.R. Schaibley, J. Yan, D.G. Mandrus, W. Yao, X. Xu, Science 351 (2016) 688–691.

[11] M.S. Choi, G.-H. Lee, Y.-J. Yu, D.-Y. Lee, S.H. Lee, P. Kim, J. Hone, W.J. Yoo, Nat. Commun. 4 (2013) 1624.

[12] L. Viti, J. Hu, D. Coquillat, A. Politano, C. Consejo, W. Knap, M.S. Vitiello, Adv. Mater. 28 (2016) 7390–7396.
[13] G.C. Constantinescu, N.D.M. Hine, Nano Lett. 16 (2016) 2586–2594.
[14] S. Kuriakose, T. Ahmed, S. Balendhran,V. Bansal,S.Sriram, M.Bhaskaran, S.Walia, 2D Mater. 5 (2018) 032001.
[15] S.P. Koenig, R.A. Doganov, H. Schmidt, A.H. Castro Neto, B. Zyilmaz, Appl. Phys. Lett. 104 (2014) 103106.
[16] H. Liu, A.T. Neal, Z. Zhu, Z. Luo, X. Xu, D. Tomanek, P.D. Ye, ACS Nano 8 (2014) 4033–4041.
[17] L. Li, Y. Yu, G.J. Ye, Q. Ge, X. Ou, H. Wu, D. Feng, X.H. Chen, Y. Zhang, Nat. Nanotechnol. 9 (2014) 372–377.
[18] S. Das, M. Demarteau, A. Roelofs, ACS Nano 8 (2014) 11730–11738.
[19] L. Kou, C. Chen, S.C. Smith, J. Phys. Chem. Lett. 6 (2015) 2794–2805.
[20] B. Chakraborty, S.N. Gupta, A. Singh, M. Kuiri, C. Kumar, D.V. Muthu, A. Das, U.V. Waghmare, A.K. Sood, Electron-hole asymmetry in the electron-phonon coupling in top-gated phosphorene transistor, 2D Mater. 3 (1) (2016) 015008.
[21] J.O. Island, G.A. Steele, H.S.J. van der Zant, A. Castellanos-Gomez, 2D Mater. 2 (2015) 011002.
[22] G. Wang, W.J. Slough, R. Pandey, S.P. Karna, 2D Mater. 3 (2016) 025011.
[23] R. Fei, L. Yang, Nano Lett. 14 (2014) 2884–2889.
[24] G. Cassabois, P. Valvin, B. Gil, Inorg. Mater. 10 (2016) 262–266.
[25] Y. Cai, G. Zhang, Y.-W. Zhang, J. Phys. Chem. C 119 (2015) 13929–13936.
[26] G. Fiori, A. Betti, S. Bruzzone, G. Iannaccone, ACS Nano 6 (2012) 2642–2648.
[27] L. Ci, L. Song, C. Jin, D. Jariwala, D. Wu, Y. Li, A. Srivastava, Z.F. Wang, K. Storr, L. Balicas, F. Liu, P.M. Ajayan, Nat. Mater. 9 (2010) 430–435.
[28] H. Park, A. Wadehra, J.W. Wilkins, A.H. Castro Neto, Appl. Phys. Lett. 100 (2012) 253115.
[29] L. Ci, L. Song, C. Jin, D. Jariwala, D. Wu, Y. Li, A. Srivastava, Z.F. Wang, K. Storr, L. Balicas, F. Liu, P.M. Ajayan, Nat. Commun. 6 (2015) 7698.
[30] J. Linghu, T. Yang, Y. Luo, M. Yang, J. Zhou, L. Shen, Y.P. Feng, ACS Appl. Mater. Interf. 10 (2018) 32142–32150.
[31] J. Hafner, J. Comput. Chem. 29 (2008) 2044–2078.
[32] J.P. Perdew, K. Burke, M. Ernzerhof, Phys. Rev. Lett. 77 (1996) 3865–3868.
[33] S. Grimme, J. Antony, S. Ehrlich, H. Krieg, J. Chem. Phys. 132 (2010) 154104.
[34] S. Grimme, S. Ehrlich, L. Goerigk, J. Comput. Chem. 32 (2011) 1456–1465.
[35] J. Heyd, G.E. Scuseria, M. Ernzerhof, J. Chem. Phys. 118 (2003) 8207.
[36] J. Paier, M. Marsman, K. Hummer, G. Kresse, I. Gerber, J.G. Angyan, J. Chem. Phys.124 (2006) 154709.
[37] P. Rivero, C.M. Horvath, Z. Zhu, J. Guan, D. Tomanek, S. Barraza-Lopez, Phys. Rev.

B 91 (2015) 115413.
[38] Z. Liu, J.Z. Liu, Y. Cheng, Z. Li, L. Wang, Q. Zheng, Phys. Rev. B 85 (2012) 205418.
[39] O.L. Blakslee, D.G. Proctor, E.J. Seldin, G.B. Spence, T. Weng, J. Appl. Phys. 41 (1970) 3373–3382.
[40] Z. Zhang, G. Ouyang, ACS Appl. Energy Mater. 1 (2018) 5675–5684.
[41] T. Kaewmaraya, P. Srepusharawoot, T. Hussian, V. Amornkitbamrung, ChemPhysChem 19 (2018) 612–618.
[42] F. Prins, A.J. Goodman, W.A. Tisdale, Nano Lett. 14 (2014) 6087–6091.
[43] L. Huang, N. Huo, Y. Li, H. Chen, J. Yang, Z. Wei, J. Li, S.-S. Li, J. Phys. Chem. Lett. 6 (2015) 2483–2488.
[44] L. Li, et al., Nat. Nanotechnol. 12 (2017) 21–25.
[45] H. Park, A. Wadehra, J.W. Wilkins, A.H.C. Neto, Appl. Phys. Lett. 100 (2012) 253115.
[46] P.G. Moses, M. Miao, Q. Yan, C.G. Van de Walle, J. Chem. Phys. 134 (2011) 084703.
[47] Y. Deng, Z. Luo, N.J. Conrad, H. Liu, Y. Gong, S. Najmaei, P.M. Ajayan, J. Lou, X. Xu, P.D. Ye, ACS Nano 8 (2014) 8292–8299.
[48] J. Dai, X.C. Zeng, J. Phys. Chem. Lett. 5 (2014) 1289–1293.
[49] P. Rivera, J.R. Schaibley, A.M. Jones, J.S. Ross, S. Wu, G. Aivazian, P. Klement, K. Seyler, G. Clark, N.J. Ghimire, J. Yan, D. Mandrus, W. Yao, X. Xu, Nat. Commun. (2015) 6242.
[50] Y. Liu, Z. Qiu, A. Carvalho, Y. Bao, H. Xu, S.J.R. Tan, W. Liu, A.H. Castro Neto, K.P. Loh, J. Lu, Nano Lett. 17 (2017) 1970–1977.
[51] M. Bernardi, M. Palummo, J.C. Grossman, ACS Nano 6 (2012) 10082–10089.
[52] M. Scharber, D. Muhlbacher, M. Koppe, P. Denk, C. Waldauf, A.J. Heeger, C. Brabec, Adv. Mater. 18 (2006) 789–794.
[53] J. Nelson, The Physics of Solar Cells, Imperial College Press and Distributed by World Scientific Publishing Co., 2003.
[54] J. Yang, R. Xu, J. Pei, Y.W. Myint, F. Wang, Z. Wang, S. Zhang, Z. Yu, Y. Lu, Light: Sci. Appl. 4 (2015) e312.
[55] J.-H. Choi, P. Cui, H. Lan, Z. Zhang, Phys. Rev. Lett. 115 (2015) 066403.
[56] X. Li, G. Jia, J. Du, X. Song, C. Xia, Z. Wei, J. Li, J. Mater. Chem. C 6 (2018) 10010.
[57] A. Rawat, R. Ahammed, D. Nityasagar, J. Manish, K. Mohanta, A.D. Sarkar, J. Phys. Chem. C 123 (2019) 12666–12675.
[58] X. Lv, W. Wei, C. Mu, B. Huang, Y. Dai, J. Mater. Chem. A 6 (2018) 5032–5039.
[59] A. Ramasubramaniam, D. Naveh, E. Towe, Phys. Rev. B 84 (2011) 205325.
[60] J. Qiao, X. Kong, Z.X. Hu, F. Yang, W. Ji, Nat. Commun. 5 (2014) 4457.

Appendix

This section includes the hard copy of the international paper (*Applied Surface Science*, **504** (2020), 144327) which has been committed as the mandatory output of the research project. Moreover, the hard copy of the optional manuscript which acknowledges TRF is included and this work has been under review in an international journal.

Output (Acknowledge the Thailand Research Fund)

1. International Journal Publication

   1.1 L. Ngmawongwan, P. Moontragoon, W. Jarernboon, C. Mondal, B. Pathak, and T. Kaewmaraya, *Applied Surface Science*, **504** (2020), 144327.

2. Research Utilization and Application

   The utilization and application of this project can be categorized into two aspects i) the academic merits and ii) the implied applications. The first aspect is demonstrated by an international publication in Applied Surface Science (Q1, IF = 5.1), an oral presentation in an international conference and a by-product publication currently under review in Journal of Hazardous Materials (Q1, IF = 7.4). The second aspect is that the project has proposed the novel applications of phosphorus as the building block of electronic and optoelectronic devices, i.e., field effect transistors (FETs), photosensors, chemical gas sensors. These applications are beyond the conventional picture of phosphorus which naturally occurs as phosphate rocks abundantly available in many provinces and is used for producing agricultural fertilizer.

3. The academic merit of this project

   This project was presented in an international conference International Conference on Surfaces, Coatings and Nanostructured Materials, December (2019) Abu Dhabi, UAE as shown by the invitation letter and some the photos below.

September 24, 2019

NANOSMAT-Middle East 2019

Thanayut Kaewmaraya
Khon Kaen University, Thailand
Thailand

Email: middleeast@nanosmat.co.uk
Web: www.nanosmat.co.uk/middleeast

Re: Abstract Acceptance – NANOSMAT-Middle East 2019 "International Conference on Surfaces, Coatings and Nanostructured Materials" - 15-17 December 2019, Abu Dhabi Polytechnic, UAE

Abstract Code: NANO-5

Dear **Thanayut Kaewmaraya**,

I am pleased to inform you that your recently submitted abstract has been accepted, after peer-review, for **Oral** presentation at the **Middle East' International Conference on Surfaces, Coatings and Nanostructured Materials (NANOSMAT-Middle East)** to be held at the Abu Dhabi Polytechnic, UAE during 15-17 December 2019. Following is the title of your accepted paper:

"BlackP Phosphorene-borocabonitride van der Waals Heterointerfaces for Promising Nanodevice Applications"

Please **remember** to mention your above abstract code (NANO-5) in any communication with the conference organizers concerning your above work and you will need to mention this when registering yourself for this conference.

This letter can also be used to obtain the necessary VISA allowing you entry to Abu Dhabi, UAE for the **NANOSMAT-Middle East** conference.

Looking forward to welcoming you to Abu Dhabi, UAE in December.

Professor Saud Aldajah
Chairman, **NANOSMAT-Middle East 2019**
Head, Electromechanical Engineering Technology
Abu Dhabi Polytechnic, P.O. Box 111499, Abu Dhabi, United Arab Emirates
Tel: 971-2-6951064; Email: saud.aldajah@adpoly.ac.ae


INTERNATIONAL CONFERENCE
EMET

Applied Surface Science 504 (2020) 144327

Contents lists available at ScienceDirect

Applied Surface Science

journal homepage: www.elsevier.com/locate/apsusc

Full Length Article

Novel BCN-phosphorene bilayer: Dependence of carbon doping on band offsets for potential photovoltaic applications

Lappawat Ngamwongwan[a], Pairot Moontragoon[b,c], Wirat Jarernboon[b,c], Chiranjit Mondal[d], Biswarup Pathak[d,e], Thanayut Kaewmaraya[b,c,*]

[a] School of Physics, Institute of Science, Suranaree University of Technology, Nakhon Ratchasima 30000, Thailand
[b] Department of Physics, Faculty of Science, Khon Kaen University, Khon Kaen 40002, Thailand
[c] Institute of Nanomaterials Research and Innovation for Energy (IN-RIE), Research Network of NANOTEC- KKU (RNN), Khon Kaen University, Khon Kaen 40002, Thailand
[d] Discipline of Metallurgy Engineering and Materials Science, Indian Institute of Technology Indore, Simrol, Indore 453552, India
[e] Discipline of Chemistry, Indian Institute of Technology (IIT) Indore, Indore, M.P. 453552, India

ARTICLE INFO

Keywords:
Two-dimensional van der Waals heterostructures
Phosphorene
Photovoltaics

ABSTRACT

Two-dimensional van der Waals heterostructures (vdWHs) have rapidly become a paradigm shift in designing high-performance electronic and optoelectronic devices. Based on the density functional theory calculations, this work presents the electronic and optical properties of novel vdWHs constituted by ternary BC_xN (x = 0, 2, and 6) and black phosphorene (BlackP). The findings reveal that BN-BlackP and BC_2N-BlackP hybrids exhibit straddling type-I band offset, whereas BC_6N-BlackP adopts staggered type-II. This compositional dependence on band alignment is ascribed to the reduction in band gaps of BC_xN upon increasing carbon concentration. The hybrids also show modulation in band gaps and band alignments caused by the external electric field due to the Stark effect. Their gaps do not only drop with the increasing field magnitude, but the band alignments also get changed. Moreover, the resultant type-II offset of BC_6N-BlackP leads to further investigation into its photovoltaic application because of the spatial electron-hole decoupling. This vdWH enhances solar absorption in the majority infrared region, yielding the efficient solar-to-electricity conversion with the theoretical power conversion efficiency (PCE) up to 22.0%. The essential gate-tunabilty and exceptional PCE clearly demonstrate the feasibility of exploiting BC_xN-BlackP vdWHs as a building block in electronic and photovoltaic devices.

1. Introduction

Atomatically-thin 2D materials have played a disruptive role in materials science over the last couple of decades since the experimental debut of graphene in 2004 [1,2]. Up to present, such a considerable number of 2D crystals has been successfully created that the family of 2D materials could span the broad spectrum of solid properties ranging from insulators to superconductors [1]. This leads to a variety of major applications covering electronic and optoelectronic devices, biosensors, and energy storage and generation, to name a few [2,3]. Nevertheless, intensive attempts to fabricate new 2D materials remain on-going in order to achieve novel properties for enhancing certain functionalities. More new 2D materials will be expectedly discovered in the near future [4].

As an alternative route, integration of existing ones has emerged as an innovative paradigm to produce 2D hybrids with unusual properties not available in the isolated components [5]. The occurrence of new features stems from the superposition, intersection or cancelation of intrinsic quantum properties of the individuals [4]. Distinct 2D crystals can be assembled by two basic approaches, i.e., either lateral or vertical combination. The former requires the constituents to be lattice-matched, consequently limiting a number of eligible heterostructures. On the other hand, the latter does not necessitate the lattice-matching constrain because such heterostructures rely on the controllable vertical stacking of dissimilar layers between which weak van der Waals (vdW) interaction is primarily responsible for aggregation [6]. This scenario allows enormous combination of possibilities and the resulted hybrids are generally regarded as van der Waals heterostructures (vdWHs) [4]. The pioneering demonstration of vdWHs is fabrication of the graphene transistor on a BN substrate where the resultant transistor exhibited the improved performance (i.e., higher carrier mobility, reduced roughness, intrinsic doping and chemical reactivity) as compared to the

* Corresponding author.
E-mail address: thakaew@kku.ac.th (T. Kaewmaraya).

https://doi.org/10.1016/j.apsusc.2019.144327
Received 18 July 2019; Received in revised form 6 September 2019; Accepted 7 October 2019
Available online 23 October 2019
0169-4332/

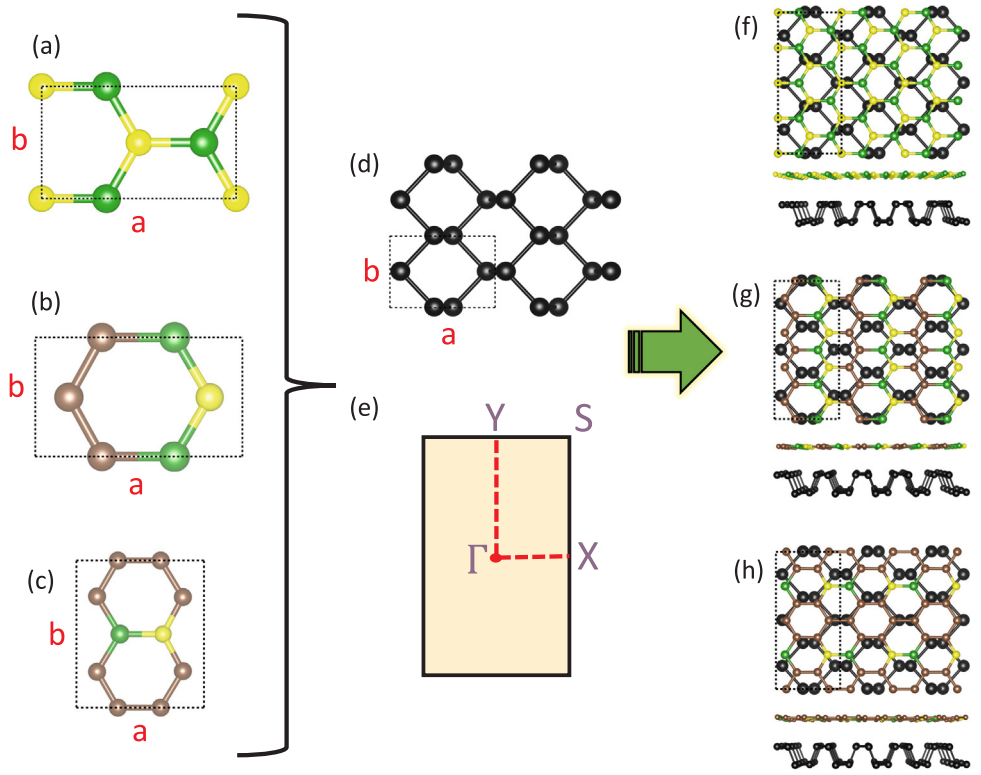

Fig. 1. Rectangular unit cell of monolayer (a) BN, (b) BC_2N, (c) BC_6N, and (d) BlackP. (e) First Brillouin zone of the orthorhombic symmetry with labeled high-symmetry points Γ(0.0, 0.0, 0.0), *X*(0.5, 0.0, 0.0), *Y* (0.0, 0.5, 0.0) and *S*(0.5, 0.5, 0.0). The unit cells as seen from the bird's eye and side views of (f) BN/BlackP, (g) BC_2N/blackP, and (h) BC_6N/blackP bilayer vdWHs. The boron, carbon, nitrogen and phosphorus atoms are represented by the green, brown, yellow, and black spheres, respectively.

traditional devices on SiO_2 [7]. Afterwards, generic vdWHs have become a feasible platform for both exploring fundamental physics and tailoring electronic and optical properties of 2D materials [4]. Notable examples include ballistic transport at a micrometer scale in graphene-BN heterostructures [8], strong light-matter interaction in transition metal dichalcogenides (TMDCs)/graphene [9], valley-polarized excitons in WSe_2-$MoSe_2$ vdWHs [10], graphene/MoS_2 tunnelling transistors [11], ultra-responsive photodetectors made from hybrid BN-2D black phosphorene [12,13]. In particular, the concept of vdWHs can resolve the so-called air-degradation of two-dimensional phosphorus [12,14].

Phosphorus can be found in various polymorphs (e.g., white, red, violet and black) of which black phosphorus is the most stable form. Although it was discovered over a century ago, mechanical exfoliation to become the few-layer form (named black phosphorene or BlackP hereafter) was recently realised in 2014 with the demonstration of the ambipolar field effect ensuing the exceptional performance in field effect transistors (FETs) [15–17]. Unlike semi-metallic graphene, BlackP is a direct-gap semiconductor enabling the ultra-high drain current on-off ratio (~10^5) [15–17]. Its gap size also covers visible to near-infrared light spectrum [18] and it is adjustably thickness-dependent, ranging from 0.3 eV in bulk to around 1.73 eV in monolayer [19]. The topology of the direct band gap remains preserved regardless of thickness, unlike in TMDCs. Furthermore, two-dimensional phosphorus possesses the greater electronic transport (carrier mobility of 1000 $cm^2\ V^{-1}\ s^{-1}$ at room temperature) which is also directionally anisotropic along the zigzag and arm-chair directions [16,20]. These exceptional features render BlackP to be an appropriate material for high-performance electronics and optoelectronic devices such as FETs, ultra-sensitive photodetectors, thermoelectric generators, and solar cells [19].

However, BlackP rapidly degrades to an insulating phosphorus oxide within a few hours under ambient conditions, consequently losing its overall attractiveness [14,21,22]. The severe oxidation process is basically attributed to the intrinsic wave-like crystal morphology and sp^3 bonding character [23]. Each phosphorus atom is covalently bonded with 3 neighbouring atoms, leaving the lone-paired electrons to be chemically prone to oxidation. This oxidative degradation can be circumvented by making vdWHs in which the atomically smooth and air-insusceptible BN is exploited as the protective layers. The use of BN is advantageous because of being a large-gap insulator (5.90 eV) [24] with relatively less amount of dangling bonds and charge traps [7]. As a result, the environmental stability of BlackP in BN-BlackP vdWHs is prolonged yet its electronic properties remains unperturbed due to the weak vdW interaction [25]. Despite being the capping layer, one can further anticipate the novelty of BN-BlackP vdWHs when the protective material is substitutionally doped by C to form new BC_xN-BlackP (x = 0, 2, and 6) hybrids. This concept is inspired by the compositional dependence on electronic properties of ternary borocarbonitrides (BC_xN) of which their band gaps get reduced gradually upon the increasing carbon concentration (from 5.90 eV in BN [24] to 0.98 eV in BC_6N) [26–29]. Hence, such vdW heterostructures of BC_xN and BlackP can be promising for two reasons, i.e., (i) retaining the air-stability of BlackP and (ii) permitting freedom to tune the electronic and optoelectronic properties of these vdWHs. The latter point is an intriguing space for further elucidation to enable targeted applications.

This work aims at unravelling the electronic and optical properties of BC_xN-BlackP (x = 0, 2, and 6) bilayer van der Waals hybrids by means of first-principles density functional theory (DFT) calculations. The key fundamental properties, including band structures, chemical bonding, band alignments, and the variation of band offsets under the influence of external electric field of these hybrids are studied. Furthermore, the prospective exploitation of these vdWHs in solar cell applications are examined through computing the absorbance and subsequently estimating the solar power conversion efficiency. The findings manifest that the band alignment of BC_xN-BlackP vdWHs are the function of carbon concentration and the external electric field (i.e.,

the tunable transition from type I to type II band offset at the appropriate concentration and field strength). In particular, type-II offset in BC_6N/BlackP can intensify solar absorption in the majority infrared regime, resulting in the exceptional photovoltaic performance.

2. Models and methods of calculations

Modelling of BC_xN-BlackP bilayer vdWHs was based on the original unit cells of BN, BC_xN [26], and BlackP. The cells of BN and BC_xN are hexagonal, whereas that of BlackP is orthorhombic. However, nominal rectangular unit cells were created to circumvent the lattice dissimilarity as shown in Fig. 1(a–d) with the orthorhombic first Brillouin zone shown in Fig. 1(e). The lattice constants of the unit cells representing (BN/BlackP), (BC_2N/BlackP), and (BC_6N/BlackP) heterostructures are (a = 4.571 Å, b = 9.927 Å, c = 30 Å), (a = 4.519 Å, b = 9.991 Å, c = 30 Å), (a = 4.593 Å, b = 9.901 Å, c = 30 Å) as displayed in Fig. 1(f–h). Although these cells internally impose the infinitesimal in-plane strain to BC_xN and BlackP sheets, the use of such lattice parameters is physically valid. This is because the computed band alignments of isolated BC_xN and BlackP in these sets of rectangular cells resemble those of the original cells. Note that the fictitious strain is an unavoidable theoretical artifact in building vdWHs to minimise the strain. However, it is not required in real devices owing to the weak vdW interaction between the monolayers [30]. The optimal interlayer distances between the monolayers were estimated by fitting the binding energy (E_b), $E_b = E_{BC_xN\text{-BlackP}} - (E_{BC_xN} + E_{BlackP})$, as a function of the interlayer distance (r) to Lennard-Jones (LJ) potential, $U_{LJ} = 4\varepsilon\left[\left(\frac{\sigma}{r}\right)^{12} - \left(\frac{\sigma}{r}\right)^{6}\right]$, where ε and σ are the fitting parameters. The first term in LJ potential accounts for repulsion, whereas the second term describes attraction. Different stacking patterns of each BC_xN-BlackP were considered and the structures with the lowest binding energies have been subsequently chosen for further investigation.

DFT-based *ab-initio* calculations were performed using VASP code [31]. The exchange correlation energy was treated by the gradient-corrected approximation according to Perdew Burke-Ernzerhof (PBE) formalism [32]. Weak vdW interaction between BC_xN and BlackP sheets was considered by incorporating the pairwise dispersive correction in the Kohn-Sham energies using the DFT-D3 approach [33,34]. The energy cutoff for the plane-wave basis set was set to 500 eV. The first Brillouin zone was sampled by Monkhorst-Pack scheme with k-mesh of $15 \times 7 \times 1$ and $17 \times 9 \times 1$ for structural optimisation and optical absorption, respectively. Structural optimisation was satisfactorily terminated when Hellmann-Feynman forces exerting on each atom were less than 10 meV/Å. The tolerance of electronic self-consistency cycle was set to 1×10^{-6} eV. The accurate determinations of band structures and optical absorption of the selected systems were carried out using hybrid Heyd-Scuseria-Ernzerhof (HSE06) functional [35,36]. However, the findings presented here were obtained from PBE functional, unless stated otherwise.

3. Results and discussion

3.1. Interlayer binding energies of vdWHs

Fig. 2(a) shows the interlayer binding energies of vdWHs as a function of the interlayer spacing. The optimal distance of BN-BlackP is 3.53 Å with a minimum binding energy of 25.95 meV/atom. These values are consistent with the reported theoretical findings in spite of the insignificant deviation inherited from the dissimilar approaches used to describe vdW forces [25,37]. The weak magnitude of binding energy and the long interlayer distance manifest the principal role of vdW interaction caused by the instantaneous dipole from charge fluctuation. The obtained fitting parameters ε and σ according to LJ formalism are 24.95 meV/atom and 2.95 Å, respectively [25]. This interlayer binding energy is slightly weaker than the measured value of graphite (30.4 meV/atom [38]), implying its relative exfoliation energy with respect to graphite. Furthermore, the binding energy as a function of the interlayer spacing allows us to estimate the elastic constant (C_{33}) in the perpendicular direction of BN and BlackP interface using the following expression, $C_{33} = \frac{r_0}{A}\frac{\partial^2 E_b(r)}{\partial r^2}$, where r_0 is the equilibrium interlayer distance, A represents the in-plane surface area of the vdWH supercell and E_b is the binding energy. The calculated C_{33} is 33.10 GPa, slightly less incompressible than that of graphite, 36.50 GPa [39]. The reason can be attributed to the fact that the wave-like geometry of BlackP results in the a large flexibility along both the horizontal and the vertical directions [25].

Meanwhile, the presence of substitutional carbon dopants in BN relatively decreases the interlayer distances, leading to the increase in binding energies despite the non-monotonic trend. The equilibrium distances (maximum binding energies) of BC_2N-BlackP and BC_6N-BlackP vdWHs amount to 3.37 Å (−30.195 meV/atom) and 3.43 Å (−27.860 meV/atom), respectively. The calculated binding energies are quantitatively comparable to that of graphite, reflecting that the peeling (exfoliation) energies of these hybrids are of nearly the same strength. The fitting parameters ε and σ of BC_2N-BlackP (BC_6N-BlackP) hybrid are −31.083 (−28.950) meV/atom and 2.79 (2.83) Å, respectively. The estimated C_{33} elastic constant of BC_2N-BlackP (BC_6N-BlackP) hybrid is 42.70 (36.20) GPa, indicating that the addition of carbon atoms makes the vdWHs less compressible. Furthermore, Fig. 2(b) depicts the plane-average potential (V_{ave}) which basically describes the combination of Hartree ($V_{Hartree}$), exchange-correlation (V_{xc}), and external (V_{ext}) potentials. Apparently, there are potential drops across the interfaces to create the built-in electric fields between the constituent sheets, yielding the spontaneous polarisation [40]. These intrinsic fields are triggered by the fundamental differences in electronegativity of B (2.01), C (2.50), N (3.07) and P (2.06) atoms and they point from BlackP to BC_xN resembling our previous work of BC_xN-Blue phosphorene interface [41]. Hence, the excitonic behaviour of vdWHs (i.e., the optical properties) tends to differ from that of individual quasi-monolayer BlackP and BC_xN due to the typically reduced dielectric screening in 2D materials [16].

3.2. Electronic structures

Fig. 3(a–d) depicts the orbitally-resolved band structures of BlackP, BN, BC_2N, and BC_6N as calculated by PBE and HSE06 levels of theory. The band gap of BlackP by PBE (HSE06) is 0.91 (1.55) eV. The HSE06 gap agrees with the reported DFT calculations [25,42,43] and close to the experimental value of 1.73 eV [44]. In particular, BlackP shows a direct-gap feature at Γ. Both the valence and conduction band extrema are formed by P-$3p_z$ orbital where the band curvature (i.e., carrier effective masses) along $\Gamma - X$ greatly differs from that along $\Gamma - Y$. This indicates that π bands derived from interactions between P-$3p_z$ orbitals contribute to direction-dependence and exceptional carrier mobility of this 2D phosphorus.

On the other hand, BN is a huge band gap (direct) insulator at K with the calculated gap of 4.65 (5.65) eV by PBE (HSE06), of which the HSE06 gap is slightly smaller than the experimental value of 5.91 eV [24]. The valence and conduction band edges are predominantly contributed by π bands from N-$2p_z$ and B-$2p_z$, respectively. The dispersion of conduction band along $M - K$ is virtually flat. This scenario leads to the difficulty in unambiguously classifying BN as either a direct-gap or an indirect-gap insulator owing to the influential role of immense excitonic binding energy in the absorption onset [24]. Meanwhile, it is found that substitutional doping of carbon in BN drastically reduces the gap. The band structure of BC_2N attests the semiconducting character with a direct PBE (HSE06) gap of 1.60 (2.19) eV at the zone center. In particular, the edge states are σbands derived from the enhanced planar overlap between B-2($p_x + p_y$) and C-2($p_x + p_y$) for the valence band edge and N-2($p_x + p_y$) and C-2($p_x + p_y$) for the conduction band edge.

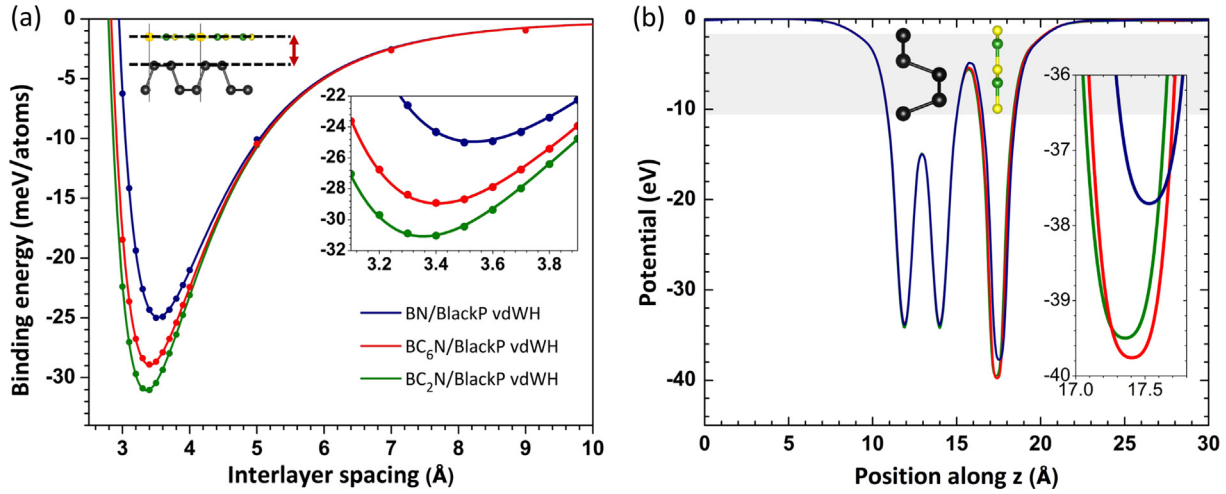

Fig. 2. (a) Interlayer binding energy (E_b) per atom of BC_xN-BlackP vdWHs as a function of the interlayer spacing which is defined as the difference in spatial coordinates in c direction between the top-most atom of BlackP and the bottom-most atom of BC_xN. The inset magnifies E_b close to the optimal points. (b) The plane-average potential along the vertical interface between BC_xN and BlackP and the inset which enlarges the potentials of BC_xN near the minimum points.

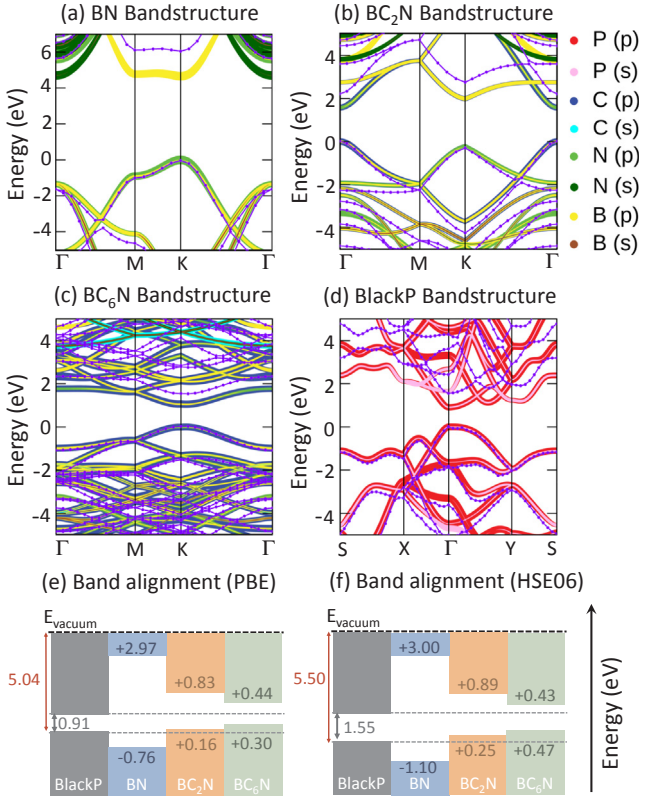

Fig. 3. Orbitally-resolved band structures of (a) BN, (b) BC_2N, (c) BC_6N, and (d) BlackP where the Fermi level is set to zero. The solid violet lines represent band dispersion calculated by HSE06 functional. Band alignments calculated by (e) PBE and (f) HSE06 functionals in which the Fermi energies are referenced to the vacuum level. The red numbers denote the calculated work functions.

This results in the significant drop in the gap at Γ. Nevertheless, the band edges at K, like BN, still show π-character where the valence (conduction) band extremum is contributed by N-$2p_z$ (B-$2p_z$). At higher doping concentration, BC_6N possesses the cone-like direct PBE (HSE06) gap of 1.04 (1.51) eV at K, whereas its Γ-gap is considerably greater. This is attributed to the fact that BC_6N is in the heavily doped regime where its band structure approaches that of graphene. The HSE06 gap of BC_6N suitably falls into the infrared region which is the majority of solar spectrum. Moreover, our spin-polarised calculations assure that BC_2N and BC_6N are nonmagnetic. This is because the simultaneous replacement of B and N sites by C atoms within the interaction length (around 10 Å) eradicates spin-splitting of the impurity states to adopt the $S = 0$ configuration [45].

The band gaps of BC_xN do not only drop with the increasing carbon concentration, but their band edge positions also get changed accordingly. This further motivates us to elucidate the band alignment when they actually form vdWHs with BlackP. Fig. 3(e–f) show the PBE and HSE06 band alignment diagrams of the isolated BC_xN and BlackP prior to forming vdWHs. The alignment is obtained by calculating the work functions of materials (W), $W = E_{vac} + E_F$, where E_{vac} and E_F represent the vacuum level and the Fermi energy, respectively. The diagrams imply that the formation of BN-BlackP vdWH yields straddling type-I band offset [25]. On the contrary, BC_xN-BlackP composites adopt type-II band offset. The band alignments from PBE and HSE06 are similar despite the differences in the gaps and work functions, manifesting that relative band alignments are less functional dependent [46]. Notably, the valence band offsets between BlackP and BC_xN are infinitesimal that the prominent interlayer couplings when forming vdWHs potentially alters the offsets.

Fig. 4(a–c) show the projected band structures, the band alignment diagram, and the charge density of valence and conduction band edges of BC_xN-BlackP vdWHs. It is evident that BN-BlackP and BC_2N-BlackP hybrids form type-I band alignment, while BC_6N-BlackP differently adopts type-II. Intriguingly, the band alignment of BC_2N-BlackP vdWH differs from that in Fig. 3(e–f). Moreover, the valence and conduction band edges of BC_6N-BlackP are now populated by BlackP and BC_6N, respectively, differing from the prior band positions in Fig. 3(e–f). The valence bands of BlackP and BC_6N in the vdWH now equalises because of the overlap among P-$3p_z$, N-$2p_z$, and C-$2p_z$ orbitals. In particular, BC_6N-BlackP exhibits type-II offset at Y-point which is preferable for optoelectronics and photovoltaics because of the spontaneously spatial separation of electrons and holes [47,48]. Further calculations of band structure and band alignment by HSE06 also yield the similar band alignment despite the difference in the gap and the offset magnitude (the conduction band offset of 0.19 eV by PBE and 0.29eV by HSE06). It is intriguing to highlight that high hole mobility in BlackP remains preserved in the BC_2N-BlackP and BC_6N-BlackP heterobilayers, as their VBM are contributed by BlackP [60]. It should be emphasised that the band realignments of BC_2N-BlackP and BC_6N-BlackP vdWHs compared with those of their isolated components are because the presence of carbon atoms intensifies the charge transfer from BlackP to BC_xN. This is apparently ascertained by the charge difference plot in Fig. 5(a).

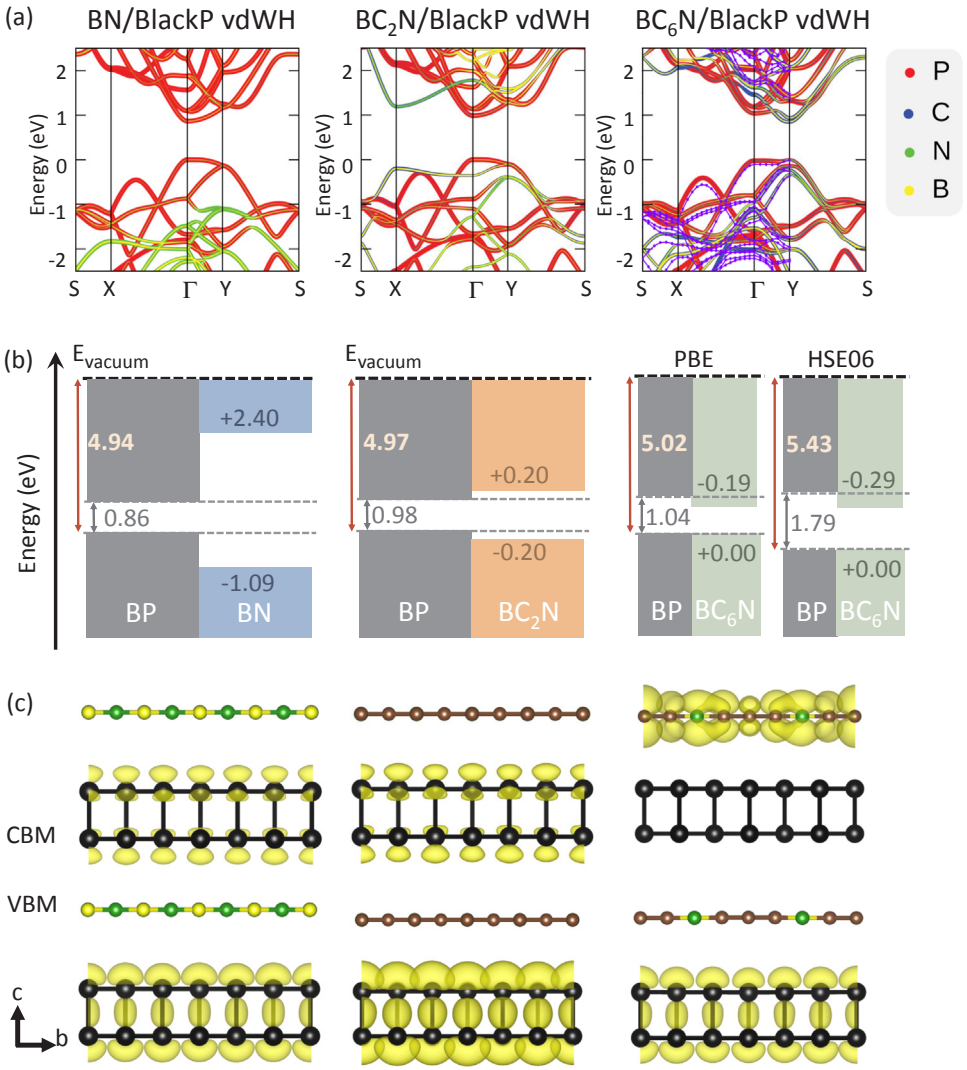

Fig. 4. (a) Projected band structures of BC_xN/BlackP vdWHs. The solid violet lines represent band dispersion calculated by HSE06 functional. Here, the valence band maximum has been shifted to zero energy. (b) The band alignment diagram and (c) the charge density of valence and conduction band edges.

There is charge accumulation (cyan) and depletion (yellow) on BC_xN and BlackP, respectively, simply because of the differences in electronegativity. Consequently, the built-in electric field gets maximised and the band positions of BlackP and BC_2N are shifted accordingly. Hence, we conclude that the built-in electric fields play a major role in the band alignment of vdWHs, especially the vdWHs constituted by the sheets with the striking difference in the electronegativities.

3.3. Effect of the electric field

Numerous studies have revealed that electronic properties of devices based on vdWHs are effectively gate-tunable (i.e., the application of back gate voltage) due to Stark effect [49,50]. The modulation of electronic and optical properties by the external electric field is beneficially reversible and non-invasive, unlike the irreversible chemical doping approach. Hence, it is intriguing to explore how BC_xN-BlackP vdWHs respond to the perturbative electric field for the possible realisation of electronic devices. Fig. 5(b-c) display the charge differences of vdWHs under the influence of the positive and negative electric fields of ± 0.5 eV/Å where the direction of positive electric field is $+c$ and vice versa. The presence of perturbation clearly causes the spatial charge redistribution. Specifically, the positive electric field induces more charge transfer from BlackP to BC_xN because the external field constructively superimposes on the built-in. Meanwhile, the negative field suppresses the charge transfer because the external field destructively reverses the built-in. More insights into the variation of band gap (E_g) of vdWHs as a function of the time independent electric field strength is shown in Fig. 5(d). Despite the different trends, the heterostructures undergo the semiconductor-to-metal transition at the same critical field magnitudes in both the directions, around -0.8 ($+0.6$) eV/Å for the negative (positive) bias. This is because their band gaps and Fermi energies of are nearly similar. Quantitatively, the PBE gaps (Fermi energies) of BN-BlackP, BC_2N-BlackP, and BC_6N-BlackP are 0.86 (-1.986), 0.98 (-1.896), and 0.85 (-1.986) eV, respectively. The phase transition facilitates the enormous tunnel current during the appropriate bias, whereas the current is comparatively less in the lack of bias, leading to the on-off ratio. In terms of the trends, the gap of BN-BlackP vdWH exhibits the plateau in the range -0.6 to $+0.6$ eV/Å where the band gap is field-independent. Unlike BN-BlackP, the reduction in band gaps of BC_2N-BlackP and BC_6N-BlackP hybrids exhibits the asymmetric quadratic Stark effect regardless of the direction, resembling the gate tunability in few-layer black phosphorus [50] and BlackP-MoS_2 vdWH [48].

The changes in the gaps of vdWHs under the influence of electric field rely on the positions of band edges. Fig. 6 shows the responsive trace of the band edges of BC_2N-BlackP and BC_6N-BlackP under the influence of the electric field from 0 to ± 0.4 eV/Å. The findings reveal that the frontier states behave differently, depending on the high-

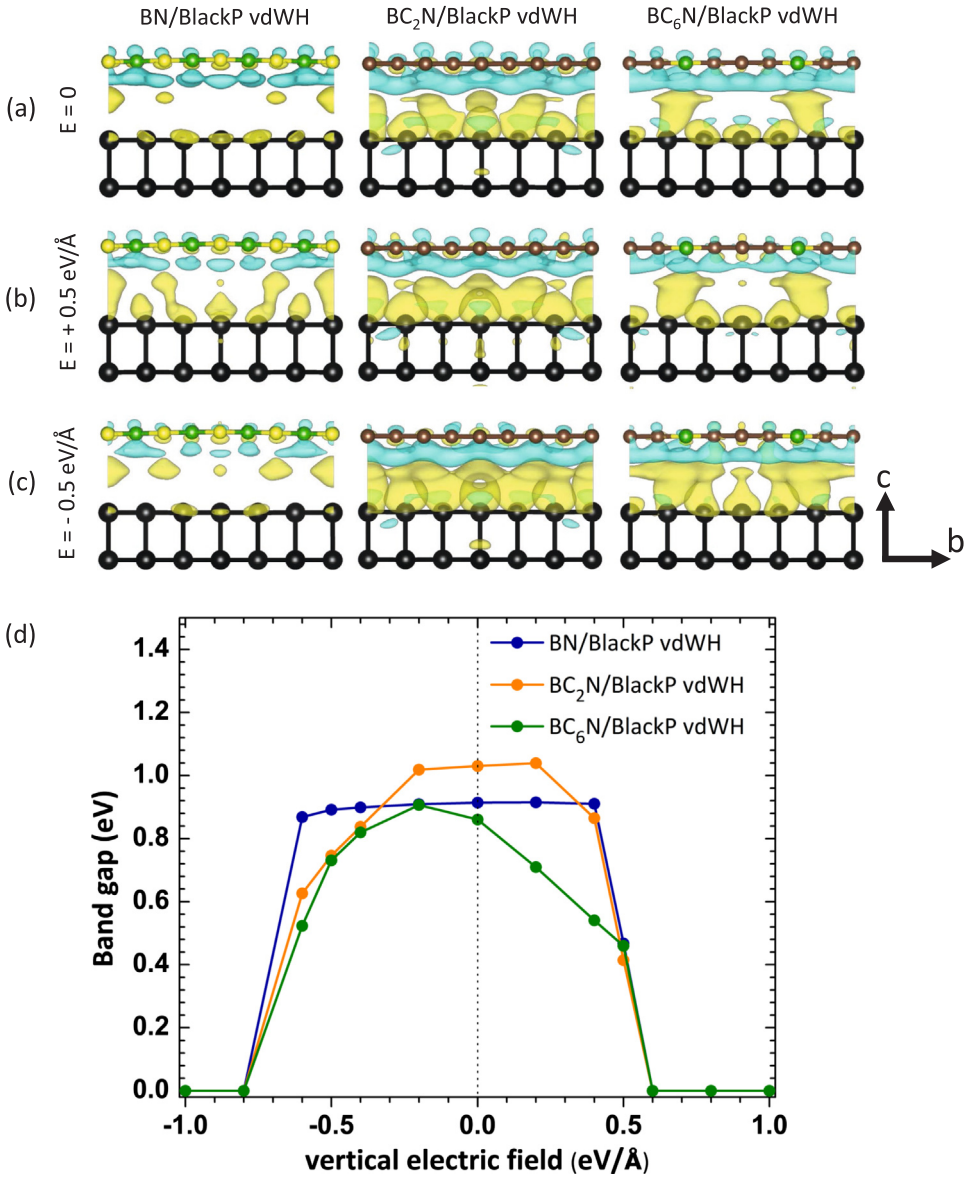

Fig. 5. The charge density difference (ρ_{diff}), $\rho_{diff} = \rho_{BC_XN-BlackP} - (\rho_{BC_XN} + \rho_{BlackP})$ of vdWHs of (a) E-field = 0.0 eV/Å, (b) E-field = +0.5 eV/Å, and (c) E-field = -0.5 eV/Å. The direction of positive electric field is +c and vice versa. Cyan and yellow colors represent charge accumulation and depletion, respectively. The isosurface level is set to be 0.0002 e/Å^3. (d) Variation of band gap of BC_xN/BlackP vdWHs with respect to the vertical electric field (E-field).

symmetry directions of the first Brillouin zone. The band edges of BlackP in all the vdWHs are not responsive to the field. On the other hand, the frontier states formed by BC_2N and BC_6N (i.e., $2p_z$ orbitals of B, C, and N atoms) are sensitively shifted towards each other. As a result, the band alignment of BC_2N-BlackP can be transformed from type-I to type-II at ± 0.4 eV/Å. Likewise, type-II offset of BC_6N-BlackP is converted into type-I at ± 0.2 eV/Å, regardless the field direction. The findings indicate that the tunability of both band gap and band alignment of BC_xN-BlackP vdWHs is governed by the active responses of the $2p_z$ orbitals from BC_xN. The different responsiveness of the edge states of BC_2N and BC_6N compared with those of BlackP can be ascribed to the lifting degeneracy by the Stark effect. The greater responsiveness of the edge states of BC_2N and BC_6N is associated with their edges states which are formed by B-$2p_z$ and N-$2p_z$ and C-$2p_z$ orbitals, unlike the frontier states of BlackP which are derived from the combination of $3p_x$, $3p_y$, and $3p_z$. Consequently, the enhanced diffuse nature of the p_z orbital readily facilitates greater charge redistribution (i. e., splitting of energy levels) [59]. This envisages the effective gate-tunability of these vdWHs as a building block in nanoelectronics.

3.4. Optical absorption and the photovoltaic performance of BC_6N-BlackP vdWH

BC_6N-BlackP vdWH exhibits type-II band offset that is feasible for spatial charge separation in the photovoltaic application. One can elucidate the performance of the photovoltaic device based on this vdWH by computing solar absorption. Fig. 7(a) shows the absorption of BC_6N-BlackP vdWH, BC_6N, and BlackP. Particularly, there is the relative enhancement in absorption of vdWH at the energy around 1.50–1.80 eV compared to the independent components. The improvement is derived from the valence-to-conduction transitions from P-$3p_z$ to P-$3p_z$ at Γ and N-$2p_z$ to B-$2p_z$ at Y, see also Fig. 4(a). This is the manifestation of BC_6N/BlackP vdWH as the potential light absorber to attain more infrared lights, potentially leading to the efficient solar-to-electricity conversion. The amplified absorption further propels us to compute the power conversion efficiency (PCE, η). This quantity describes the amount of solar energy being converted to electricity and it can be theoretically estimated according to Bernadi and Scharber formalism [51,52]

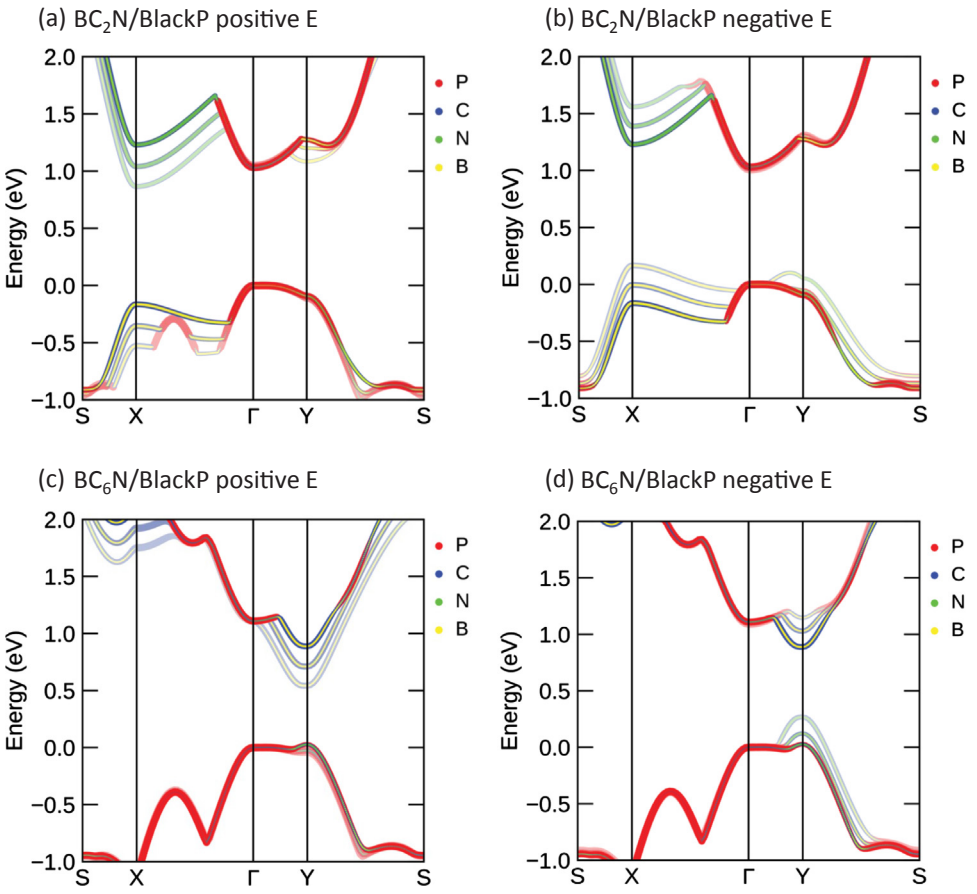

Fig. 6. (a) Relative variation of valence and conduction band edges of BC_xN/BlackP vdWHs with respect to the vertical electric field (a) BC_2N/BlackP with the field magnitude of 0.0, 0.2 and 0.4 eV/Å (b) BC_2N/BlackP with the field magnitude of 0.0, −0.2 and −0.4 eV/Å, (c) BC_6N/BlackP with the field magnitude of 0.0, 0.2 and 0.4 eV/Å, and (d) BC_6N/BlackP with the field magnitude of 0.0, −0.2 and −0.4 eV/Å.

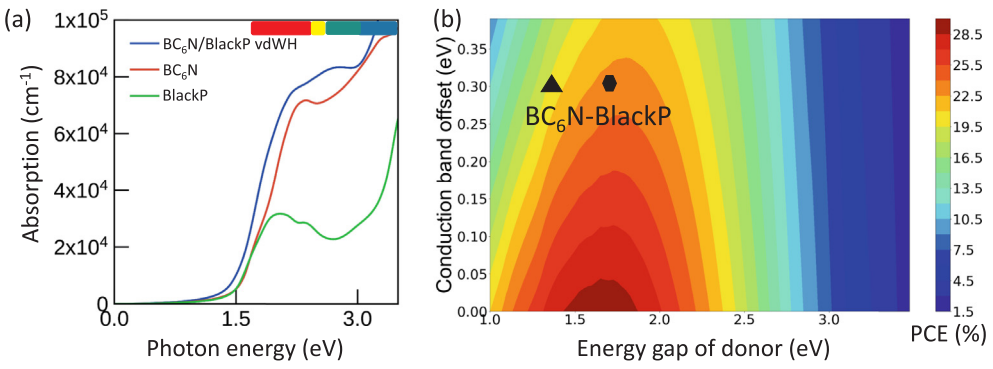

Fig. 7. (a) Absorption of BC_6N/BlackP vdWH, (b) the landscape of the power conversion efficiency (PCE) as a function of the conduction band offsets and the band gap of the donor material. The hexagonal and triangular dots represent the theoretical PCE evaluated from the electronic HSE06 and the experimental optical gap, respectively. (c) the conceptual demonstration of the solar cell made from BC_6N/BlackP vdWH.

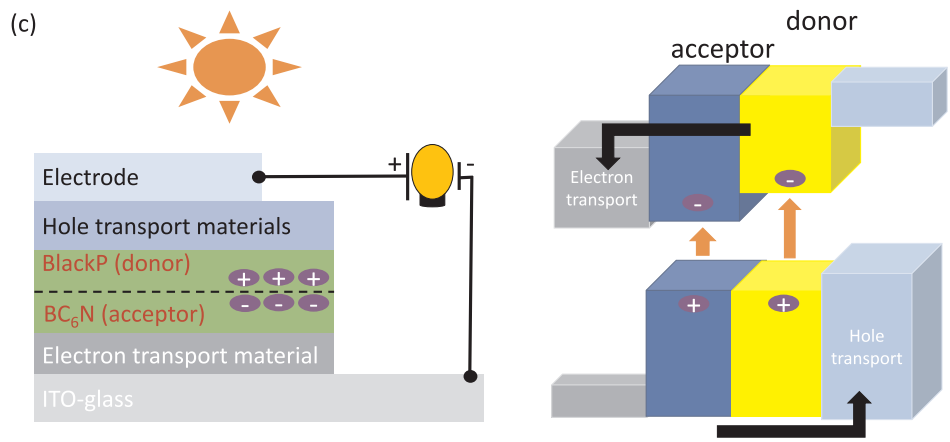

$$\eta = \frac{FF \cdot V_{OC} \cdot J_{SC}}{P_{light}} = \frac{0.65(E_g^d - \Delta E_C - 0.3)\int_{E_g^d}^{\infty} \frac{P(\hbar\omega)}{\hbar\omega} d(\hbar\omega)}{\int_0^{\infty} P(\hbar\omega) d(\hbar\omega)}$$

where *FF* is the fill factor which determines ratio between the maximum power point and the open circuit voltage and the short circuit current [53]. *FF* typically varies from 0.50 to 0.82, depending on materials, while *FF* is set to 0.65 in this study [52]. This empirical number is experimentally estimated according to the practical limit of external quantum efficiency of solar cells absorbing photon energies equal or greater than the donors' band gaps without the recombination losses [52]. Meanwhile, V_{OC} defines the estimation of highest open-circuit voltage which is expressed as $V_{OC} = E_g^d - \Delta E_C - 0.3$ (in unit of eV). E_g^d represents the optical band gap of the donor (here BlackP) which is regarded as the material with the relatively higher conduction band. ΔE_C accounts for the conduction band offset between the donor and the acceptor and the empirical factor 0.3 denotes the energy conversion kinetics. The optical band gap in the present study is approximated by the electrical band gap (i.e., Kohn-Sham band gap) at HSE06 level of theory. Although both kinds of band gap differ by the presence of exciton energy that generally makes the former smaller [54], this simplification remains reasonable due to the linear variation of exciton energy with the band gap [55]. The trend of PCE can be correctly predicted despite the systematic shift of the absolute values. J_{SC} is the short circuit current which is calculated by the integral of the energy-dependence of AM1.5 solar energy flux, $P(\hbar\omega)$ in unit of $W/m^{-2}/eV^{-1}$, weighted by photon energy $\hbar\omega$. Meanwhile, P_{light} in the denominator is the total solar power of AM1.5 solar energy flux. The integrals of J_{SC} and P_{light} were carried out by the basic Simpson approach. The comprehensive analysis of Eq. (1) tells us that either a too high or too small donor gap results in the low PCE. In addition, large ΔE retards PCE because of the thereby significant energy loss.

Fig. 7(b) depicts the dependence of the calculated PCE as a function of the conduction band offset (0.29 eV) and the band gap of the donor material (1.79 eV). BC_6N/BlackP vdWH can deliver the maximum PCE of around 22.0%, denoted by the hexagonal dot. In comparison, the experimental optical band gap taking excitons into account is 1.30 ± 0.02 eV [54] is estimated to be ca. 20.0%, denoted by the triangular dot. Considering the errors in calculating the donor's band gap is around 0.49 eV and the error in the open-circuit voltage (ΔV_{OC}) is 0.10 eV [51]. The error of PCE (α) can be evaluated as [51]

$$\alpha = \frac{1}{\eta}\sqrt{\left[\left(\frac{\partial\eta}{\partial V_{OC}}\right)\Delta V_{OC}\right]^2 + \left[\left(\frac{\partial\eta}{\partial E_g^d}\right)\Delta E_g^d\right]^2}$$

The error is calculated to be 3.0%, hence the upper bound of PCE ranging from 19.0 to 22.0%. This exceptional number is exceedingly comparable to the theoretical figures of several vdWHs such as 18.0% of BlackP-MoS_2 [48] and 23% of BAs-BlackP (high-throughput screening) [30]. The conceptual demonstration of using this vdWH as a solar absorber is schematically shown in Fig. 7(c). It should be mentioned that the theoretical PCE is solely based on the band gap and the conduction band offset. The actual PCE involves multiple factors such as transport of charge carriers, diffusion length and excitonic recombination, etc., which are not taken into account in the present work. In addition, PCE is probably less sensitive to the stacking pattern of the constituents of vdWHs because the intrinsically weak magnitude of interlayer interaction generally causes the minor changes in the atomic structures (and band gaps) of the component materials [56–58] Nonetheless, our proposed system can hopefully stimulate further in-depth investigation to entail the opportunity in alternative solar cell devices.

4. Conclusion

In summary, we present the electronic and optical properties of BC_xN-BlackP ($x = 0, 2, 6$) vdWHs investigated by means of first-principles DFT. The electronic properties of these vdWHs are effectively tunable by varying carbon concentration. BN-BlackP and BC_2N-BlackP exhibit type-I band offset whereas BC_6N-BlackP adopts type-II band offset. The variation in band alignment is ascribed to the reduction in band gaps of BC_xN upon increasing carbon concentration and the prominent interlayer interactions between the constituent monolayers. The electronic properties of vdWHs can also be modulated by the external electric field due to the fundamental Stark effect. The band gaps of these hybrids drop with the applied electric field regardless of the field direction where band alignment also gets changed. This unique modulation in gap and alignment essentially enables gate-tenability of these vdWHs as a building block in electronic FET devices. Moreover, the potential photovoltaic application of BC_6N-BlackP vdWH has been investigated because of its type-II band alignment. BC_6N BlackP vdWH enhances solar absorption in the infrared region that leads to the efficient solar-to-electricity conversion. The estimated maximum power conversion efficiency (PCE) is exceptional 19.0–22.0%. This appealing figure can hopefully stimulate experimental studies to entail the opportunity in alternative solar cell devices.

Acknowledgements

This research is financially supported by Thailand Research Fund (Grant no. MRG6180157) and the Research Fund for DPST Graduate with First Placement (Grant no. 005/2559), the Institute for the Promotion of Teaching Science and Technology (IPST), Thailand. In addition, this work has been partially supported by the Institute of Nanomaterials Research and Innovation for Energy (IN-RIE), Khon Kaen University and the National Nanotechnology Center (NANOTEC), NSTDA, Ministry of Science and Technology, Thailand, through its program of Research Network NANOTEC (RNN). T. Kaewmaraya is indebted to the academic mentoring from Prof. Vittaya Amornkitbamrung from Khon Kaen university.

References

[1] G.R. Bhimanapati, et al., ACS Nano 9 (2015) 11509–11539.
[2] A.C. Ferrari, et al., Nanoscale 7 (2015) 4598–4810.
[3] N. Briggs, et al., 2D Mater. 6 (2019) 022001.
[4] C.N.R. Rao, U.V. Waghmare, 2D Inorganic Materials beyond Graphene, WORLD SCIENTIFIC (EUROPE), 2017.
[5] D. Jariwala, A.R. Davoyan, J. Wong, H.A. Atwater, ACS Photonics 4 (2017) 2962–2970.
[6] A.K. Geim, I.V. Grigorieva, Nature 499 (2013) 419–425.
[7] C.R. Dean, A.F. Young, I. Meric, C. Lee, L. Wang, S. Sorgenfrei, K. Watanabe, T. Taniguchi, P. Kim, K.L. Shepard, J. Honel, Nat. Nanotechnol. 5 (2010) 722.
[8] A.S. Mayorov, R.V. Gorbachev, S.V. Morozov, L. Britnell, R. Jalil, L.A. Ponomarenko, P. Blake, K.S. Novoselov, K. Watanabe, T. Taniguchi, A.K. Geim, Nano Lett. 11 (2011) 2396–2399.
[9] L. Britnell, R.M. Ribeiro, A. Eckmann, R. Jalil, B.D. Belle, A. Mishchenko, Y.-J. Kim, R.V. Gorbachev, T. Georgiou, S.V. Morozov, A.N. Grigorenko, A.K. Geim, C. Casiraghi, A.H.C. Neto, K.S. Novoselov, Science 340 (2013) 1311–1314.
[10] P. Rivera, K.L. Seyler, H. Yu, J.R. Schaibley, J. Yan, D.G. Mandrus, W. Yao, X. Xu, Science 351 (2016) 688–691.
[11] M.S. Choi, G.-H. Lee, Y.-J. Yu, D.-Y. Lee, S.H. Lee, P. Kim, J. Hone, W.J. Yoo, Nat. Commun. 4 (2013) 1624.
[12] L. Viti, J. Hu, D. Coquillat, A. Politano, C. Consejo, W. Knap, M.S. Vitiello, Adv. Mater. 28 (2016) 7390–7396.
[13] G.C. Constantinescu, N.D.M. Hine, Nano Lett. 16 (2016) 2586–2594.
[14] S. Kuriakose, T. Ahmed, S. Balendhran, V. Bansal, S. Sriram, M. Bhaskaran, S. Walia, 2D Mater. 5 (2018) 032001.
[15] S.P. Koenig, R.A. Doganov, H. Schmidt, A.H. Castro Neto, B. Zyilmaz, Appl. Phys. Lett. 104 (2014) 103106.
[16] H. Liu, A.T. Neal, Z. Zhu, Z. Luo, X. Xu, D. Tomanek, P.D. Ye, ACS Nano 8 (2014) 4033–4041.
[17] L. Li, Y. Yu, G.J. Ye, Q. Ge, X. Ou, H. Wu, D. Feng, X.H. Chen, Y. Zhang, Nat. Nanotechnol. 9 (2014) 372–377.
[18] S. Das, M. Demarteau, A. Roelofs, ACS Nano 8 (2014) 11730–11738.
[19] L. Kou, C. Chen, S.C. Smith, J. Phys. Chem. Lett. 6 (2015) 2794–2805.
[20] B. Chakraborty, S.N. Gupta, A. Singh, M. Kuiri, C. Kumar, D.V. Muthu, A. Das, U.V. Waghmare, A.K. Sood, Electron-hole asymmetry in the electron-phonon coupling in top-gated phosphorene transistor, 2D Mater. 3 (1) (2016) 015008.
[21] J.O. Island, G.A. Steele, H.S.J. van der Zant, A. Castellanos-Gomez, 2D Mater. 2 (2015) 011002.
[22] G. Wang, W.J. Slough, R. Pandey, S.P. Karna, 2D Mater. 3 (2016) 025011.

[23] R. Fei, L. Yang, Nano Lett. 14 (2014) 2884–2889.
[24] G. Cassabois, P. Valvin, B. Gil, Inorg. Mater. 10 (2016) 262–266.
[25] Y. Cai, G. Zhang, Y.-W. Zhang, J. Phys. Chem. C 119 (2015) 13929–13936.
[26] G. Fiori, A. Betti, S. Bruzzone, G. Iannaccone, ACS Nano 6 (2012) 2642–2648.
[27] L. Ci, L. Song, C. Jin, D. Jariwala, D. Wu, Y. Li, A. Srivastava, Z.F. Wang, K. Storr, L. Balicas, F. Liu, P.M. Ajayan, Nat. Mater. 9 (2010) 430–435.
[28] H. Park, A. Wadehra, J.W. Wilkins, A.H. Castro Neto, Appl. Phys. Lett. 100 (2012) 253115.
[29] L. Ci, L. Song, C. Jin, D. Jariwala, D. Wu, Y. Li, A. Srivastava, Z.F. Wang, K. Storr, L. Balicas, F. Liu, P.M. Ajayan, Nat. Commun. 6 (2015) 7698.
[30] J. Linghu, T. Yang, Y. Luo, M. Yang, J. Zhou, L. Shen, Y.P. Feng, ACS Appl. Mater. Interf. 10 (2018) 32142–32150.
[31] J. Hafner, J. Comput. Chem. 29 (2008) 2044–2078.
[32] J.P. Perdew, K. Burke, M. Ernzerhof, Phys. Rev. Lett. 77 (1996) 3865–3868.
[33] S. Grimme, J. Antony, S. Ehrlich, H. Krieg, J. Chem. Phys. 132 (2010) 154104.
[34] S. Grimme, S. Ehrlich, L. Goerigk, J. Comput. Chem. 32 (2011) 1456–1465.
[35] J. Heyd, G.E. Scuseria, M. Ernzerhof, J. Chem. Phys. 118 (2003) 8207.
[36] J. Paier, M. Marsman, K. Hummer, G. Kresse, I. Gerber, J.G. Angyan, J. Chem. Phys. 124 (2006) 154709.
[37] P. Rivero, C.M. Horvath, Z. Zhu, J. Guan, D. Tománek, S. Barraza-Lopez, Phys. Rev. B 91 (2015) 115413.
[38] Z. Liu, J.Z. Liu, Y. Cheng, Z. Li, L. Wang, Q. Zheng, Phys. Rev. B 85 (2012) 205418.
[39] O.L. Blakslee, D.G. Proctor, E.J. Seldin, G.B. Spence, T. Weng, J. Appl. Phys. 41 (1970) 3373–3382.
[40] Z. Zhang, G. Ouyang, ACS Appl. Energy Mater. 1 (2018) 5675–5684.
[41] T. Kaewmaraya, P. Srepusharawoot, T. Hussian, V. Amornkitbamrung, ChemPhysChem 19 (2018) 612–618.
[42] F. Prins, A.J. Goodman, W.A. Tisdale, Nano Lett. 14 (2014) 6087–6091.
[43] L. Huang, N. Huo, Y. Li, H. Chen, J. Yang, Z. Wei, J. Li, S.-S. Li, J. Phys. Chem. Lett. 6 (2015) 2483–2488.
[44] L. Li, et al., Nat. Nanotechnol. 12 (2017) 21–25.
[45] H. Park, A. Wadehra, J.W. Wilkins, A.H.C. Neto, Appl. Phys. Lett. 100 (2012) 253115.
[46] P.G. Moses, M. Miao, Q. Yan, C.G. Van de Walle, J. Chem. Phys. 134 (2011) 084703.
[47] Y. Deng, Z. Luo, N.J. Conrad, H. Liu, Y. Gong, S. Najmaei, P.M. Ajayan, J. Lou, X. Xu, P.D. Ye, ACS Nano 8 (2014) 8292–8299.
[48] J. Dai, X.C. Zeng, J. Phys. Chem. Lett. 5 (2014) 1289–1293.
[49] P. Rivera, J.R. Schaibley, A.M. Jones, J.S. Ross, S. Wu, G. Aivazian, P. Klement, K. Seyler, G. Clark, N.J. Ghimire, J. Yan, D. Mandrus, W. Yao, X. Xu, Nat. Commun. (2015) 6242.
[50] Y. Liu, Z. Qiu, A. Carvalho, Y. Bao, H. Xu, S.J.R. Tan, W. Liu, A.H. Castro Neto, K.P. Loh, J. Lu, Nano Lett. 17 (2017) 1970–1977.
[51] M. Bernardi, M. Palummo, J.C. Grossman, ACS Nano 6 (2012) 10082–10089.
[52] M. Scharber, D. Muhlbacher, M. Koppe, P. Denk, C. Waldauf, A.J. Heeger, C. Brabec, Adv. Mater. 18 (2006) 789–794.
[53] J. Nelson, The Physics of Solar Cells, Imperial College Press and Distributed by World Scientific Publishing Co., 2003.
[54] J. Yang, R. Xu, J. Pei, Y.W. Myint, F. Wang, Z. Wang, S. Zhang, Z. Yu, Y. Lu, Light: Sci. Appl. 4 (2015) e312.
[55] J.-H. Choi, P. Cui, H. Lan, Z. Zhang, Phys. Rev. Lett. 115 (2015) 066403.
[56] X. Li, G. Jia, J. Du, X. Song, C. Xia, Z. Wei, J. Li, J. Mater. Chem. C 6 (2018) 10010.
[57] A. Rawat, R. Ahammed, D. Nityasagar, J. Manish, K. Mohanta, A.D. Sarkar, J. Phys. Chem. C 123 (2019) 12666–12675.
[58] X. Lv, W. Wei, C. Mu, B. Huang, Y. Dai, J. Mater. Chem. A 6 (2018) 5032–5039.
[59] A. Ramasubramaniam, D. Naveh, E. Towe, Phys. Rev. B 84 (2011) 205325.
[60] J. Qiao, X. Kong, Z.X. Hu, F. Yang, W. Ji, Nat. Commun. 5 (2014) 4457.